32. GEOTECHNICAL PROPERTIES OF SEDIMENTS FROM THE MIDDLE AMERICA TRENCH AND SLOPE[1]

Elliott Taylor and William R. Bryant, Department of Oceanography, Texas A&M University[2]

ABSTRACT

The geotechnical characteristics of 22 sediment samples from Leg 84 sites were studied in an effort to associate these with processes active along the Middle America slope and with sedimentation mechanisms. Geotechnical properties measured include water content, porosity, bulk density, Atterberg limits, consolidation characteristics, permeability, and vane shear strength. A majority of samples obtained from Sites 565, 568, and 570 show significant disturbance resulting from degassing. This disturbance apparently results in underconsolidation, although other mechanisms such as excess pore pressures generated from the subduction process can also contribute to this state. Overconsolidated sediments were found at Sites 565, 566, and 569. The overconsolidated sediments at Sites 565 and 569 may result from downslope transport mechanisms rearranging and stressing the sediment mass under consideration. The sediment condition at Site 566 is probably a result of eroded overburden: an estimated 87 m of overlying sediments may have been removed. Geotechnical and permeability relationships with depth are consistent with those found for other hemipelagic sediments of silty clay to clayey silt textures.

INTRODUCTION

This study describes the Leg 84 Middle America slope-sediments in the geotechnical sense, analyzing the character of physical properties, the state of consolidation, and the sediment permeability as they may relate to the processes active along this margin.

The depositional framework of sediments blanketing the Middle America Trench and slope is subject to a variety of processes, including downslope transport, erosion, and subduction-erosion. Geotechnical properties at active margins have been studied in an attempt to identify the relationship between subduction and accretion of the slope and oceanic-plate sediment piles. Shephard (1981) described several near-trench sediments in terms of their geotechnical properties and the associated subduction pattern. The Middle America Trench- and slope-sediments off Guatemala, as he concluded, are principally pelagic. The tectonic activity along this margin, coupled with sedimentation processes, the occurrence of methane hydrates, and the nature of the sediments themselves, creates, however, a setting unlike that of simple pelagic deposition. Faas (1982a, b) performed physical-properties analysis of sediments from Leg 67 along the Guatemalan margin and concluded that most geotechnical properties are dominated by *in situ* gas, sedimentation, and downslope transport.

METHODS

Physical properties measured and tabulated (see Appendix to this chapter) for the DSDP Leg 84 sites were obtained using standard methods. Shipboard analyses provided bulk density, water content, porosity, undrained shear strength, and compressional-wave velocity. The techniques for obtaining these measurements have been described by Boyce (1976). The bulk density and porosity data were obtained on the *Glomar Challenger* using the continuous and 2-min. GRAPE and gravimetric methods. Saturated-sediment conditions were assumed for porosity measurements and for GRAPE computations. GRAPE calculations also assume average grain densities of 2.65 Mg/m^3 for hemipelagic sediments, 2.70 Mg/m^3 for hard rock specimens, and a fluid density of 1.025 Mg/m^3. Compressional-wave velocity was measured in the Hamilton Frame velocimeter. Vane measurements of undrained shear strength were obtained utilizing a hand-held Torvane device and were measured perpendicular to the bedding plane on split sections. Shipboard sampling was done as often as feasible, generally yielding one data point per 2 m, or at points showing distinct lithological changes.

Shore-based laboratory measurements of physical properties include water content, Atterberg limits, bulk density, and grain density from samples taken for consolidation testing. Volumetric determinations were measured using an air-comparison pycnometer with helium as the gas medium. In addition, vane shear measurements were made using a motorized vane at a shear rate of 60°/min. All samples remaining from shipboard velocity analyses, together with those from consolidation sampling, were utilized to obtain percentage of calcium carbonate by the Schiebler technique (Bouma, 1969) and for grain-size analysis by the pipette method for silts and clays (Folk, 1974).

Consolidation and permeability tests were run with Anteus backpressured consolidometers modified for falling-head permeability measurements. Theory and procedures for standard consolidation and falling-head permeability tests are described by Lambe (1951) and Lambe and Whitman (1969). Lowe et al. (1964) point out the advantages of backpressured consolidation testing. All tests for the Leg 84 material were run with a backpressure of 675 kPa to ensure complete saturation of the sediment. Consolidation loads were step-loaded in multiples of 2 from a minimum of 3 kPa to a maximum of 3200 kPa. Permeability measurements were obtained 24 hrs. after the application of each new load, thus yielding a distribution of permeability values at various void ratios. The resultant curve produced from consolidation tests is a plot of void ratio versus effective stress (e–log P_o'). A typical curve (Fig. 1) shows a reload segment at low vertical stresses, a zone of stronger curvature, and a final linear portion reflecting the virgin curve. The curvature of the break from the reloaded position to the virgin curve is in part a function of the disturbance of the sample; undisturbed samples will generally have a better-defined break. The maximum past effective overburden pressure (P_c') was obtained using the Casagrande (1936) technique, and it represents the maximum effective vertical pressure with which the sediment had come into equilibrium. Values of P_c' exceeding the actual *in situ* effective overburden pressure (P_o') represent a state designated in soil mechanics as overconsolidation, and the opposite state would be underconsolidation (Terzaghi, 1941). The over-

[1] von Huene, R., Aubouin, J., et al., *Init. Repts. DSDP*, 84: Washington (U.S. Govt. Printing Office).

[2] Address: Department of Oceanography, Texas A&M Univ., College Station, TX 77843.

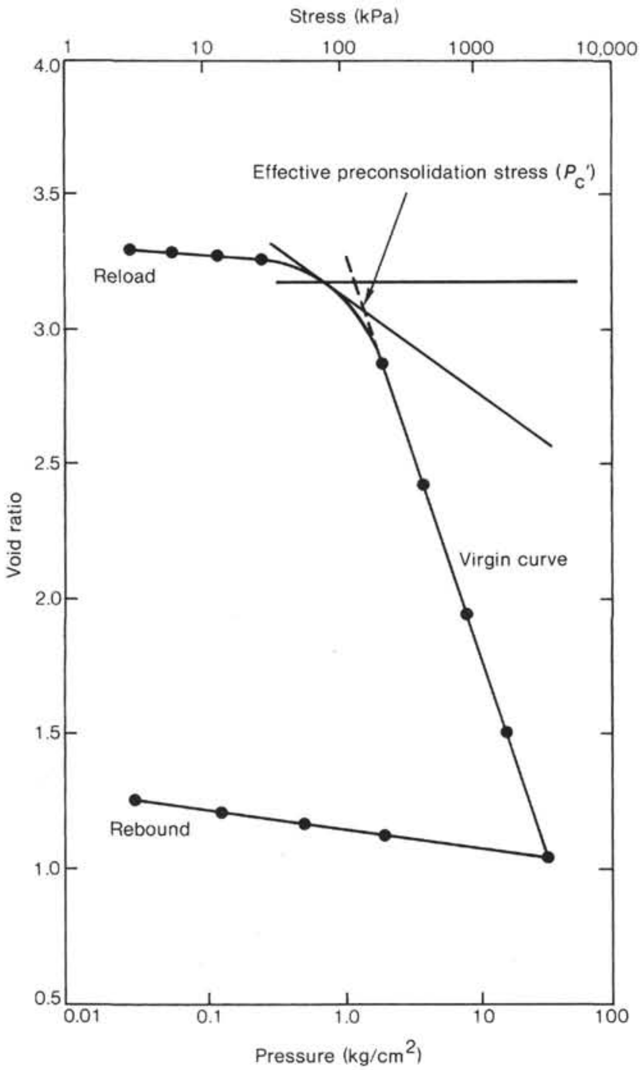

Figure 1. Typical curve of void ratio vs. log effective vertical stress (e–log P_o'), showing associated nomenclature and a representation of the Casagrande graphical solution for determining the preconsolidated effective stress.

consolidation ratio (OCR) is the ratio of P_c' to P_o', and it numerically represents the state of consolidation. An OCR of 1 reflects a normally consolidated sediment, and an OCR greater than 1 represents an overconsolidated state.

RESULTS

Site 565

The one hole drilled on the lower slope of the Costa Rican margin during Leg 84 (Fig. 2) indicated that sediments consist of 328 m of a dark, greenish gray silty clay and mudstone, the oldest sediment being lower Pliocene–upper Miocene. The sediments contained varying amounts of gas that disrupted the fabric of the recovered samples to different degrees; all samples for measurement of physical properties were selected, however, where this disturbance appeared to be minimal.

Grain-size analyses of sediments at this site show a uniform silty clay texture with depth, with only a few excursions from an overall trend of slightly increasing clay content (Fig. 3). Atterberg limits determined for two samples classify sediments in Section 565-1-4 as inorganic clay of medium to high plasticity and sediments in Section 565-10-6 as fine sand and silt of medium to high plasticity (Fig. 4).

In general, the sediment section shows a rapidly decreasing water content (60–40%) and porosity (80–65%) from surficial sediments to approximately 20 m sub-bottom, at which depth the gradients decrease significantly (Fig. 3). Water-content, porosity, and bulk-density profiles are nearly vertical below this depth. Two rather abrupt increases (10% in water content) occur at 48 and 195 m sub-bottom, possibly reflecting zones of depositional hiatuses and/or erosion, although this cannot be substantiated through biostratigraphic results.

The state of consolidation of these sediments may be estimated by using the ratio of shear strength to effective overburden (C_u/P_o'). This state can be assessed by comparing the ratio against the range of 0.2–0.5 as defined by Skempton (1970) for normally consolidated marine sediments. The C_u/P_o' ratio at Site 565 is approximately 0.70 for the upper 20 m, suggesting that these sediments are slightly overconsolidated. Below 20 m the overall trend averages 0.22, suggesting normally to slightly underconsolidated sediments.

Two laboratory consolidation tests were performed on sediments from this site; the results are summarized in Table 1 and Figure 5. The preconsolidation stresses (P_c') for these two samples are well defined, and suggest that these samples are slightly underconsolidated (Section 565-1-4) to very underconsolidated (Section 565-10-6). Section 565-10-6 consists of a mud and mudstone mixture with high contents of sand and silt, which may be responsible, to some degree, for a low OCR value. Section 565-1-4 shows a moderate degree of compressibility, represented by the compression index (C_c) value of 1.22, whereas Section 565-10-6 has a low compressibility ($C_c = 0.67$), reflecting the effects of sand-to silt-size material on compression.

The discrepancy in the state of overconsolidation between the C_u/P_o' results for the upper 20 m and the laboratory test for Section 565-1-4 may result from comparing a downhole trend, as in the case of undrained shear strength versus overburden, to a defined point in the sediment column, such as the consolidation sample. The environment of deposition on the Costa Rican slope is prone to considerable downslope mass-transport mechanisms that may, in fact, create a variable trend in consolidation behavior (see Baltuck et al., this volume).

Permeability results for the two consolidation samples from Site 565 are shown in Table 1. These permeabilities are interpolated estimates corresponding to the void ratio of the sediment at its preconsolidation stress. Permeability thus estimated is most likely to approach the *in situ* vertical permeability of the sediment. Permeabilities on the order of 10^{-7} cm/s, represent typical values for silty clays when compared with other marine sediments (Bryant et al., 1981), and such values would be interpreted as indicating sediments with a very low degree of permeability (Terzaghi and Peck, 1967).

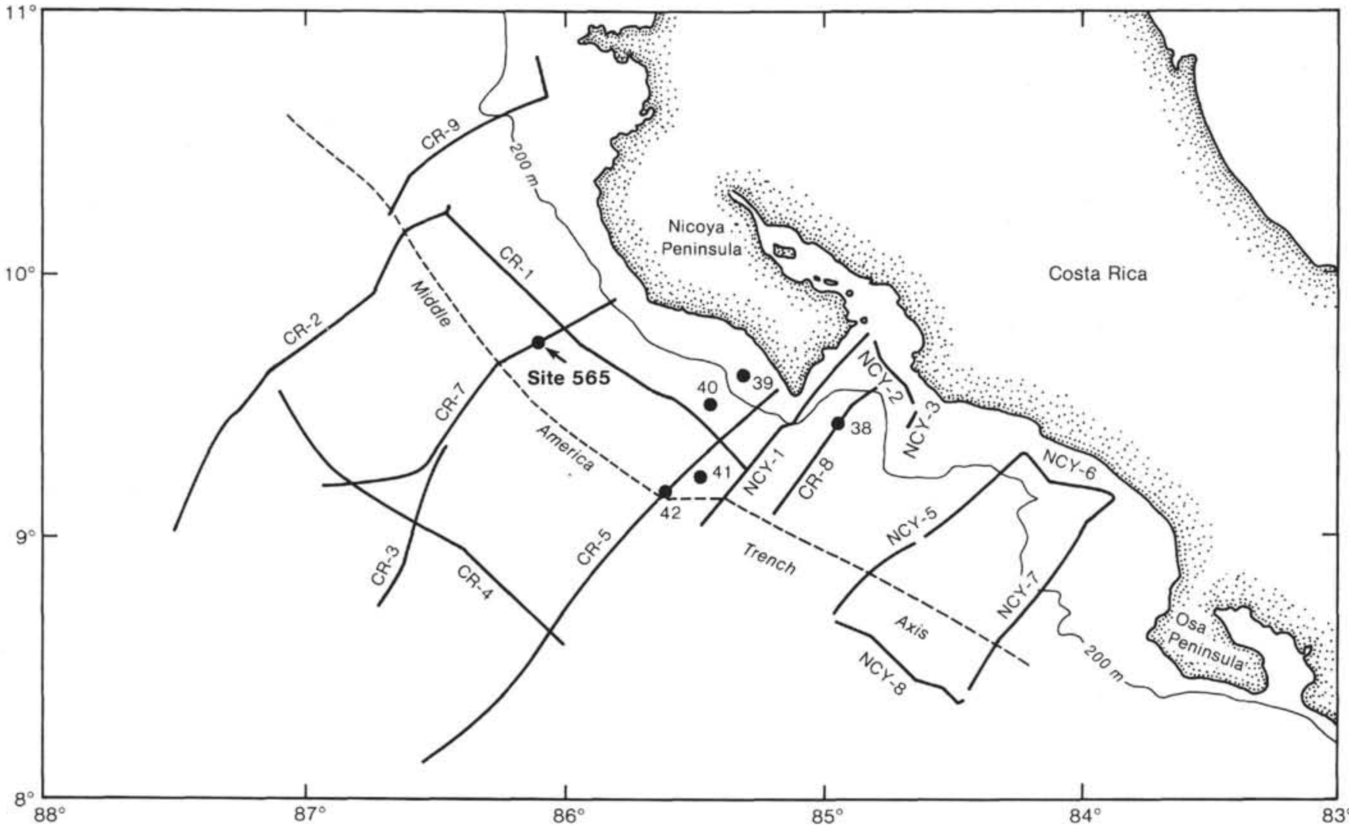

Figure 2. Location of DSDP Site 565.

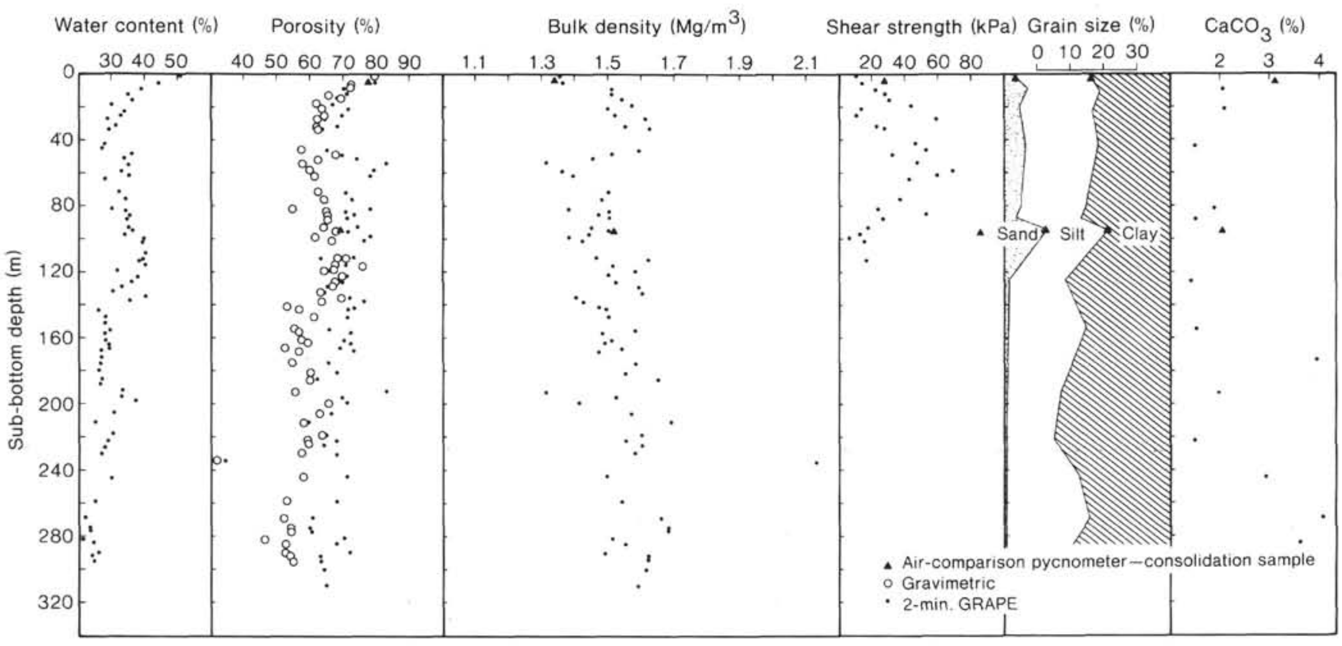

Figure 3. Geotechnical properties of sediments from Site 565.

Site 566

Site 566 is on the Middle America Trench slope, on the flank of the San José Canyon (Fig. 6). This site has a very thin sediment cover consisting principally of dark, olive-gray siliceous mud. The grain-size analyses for these sediments classify them as silty clays, and the Atterberg limits for one sample representative of the column classify them as borderline between inorganic clays or fine sands and silts of medium to high plasticity (Fig. 4).

The general trend in index properties shows a gradual increase in bulk density (1.43–1.66 Mg/m^3) and decreas-

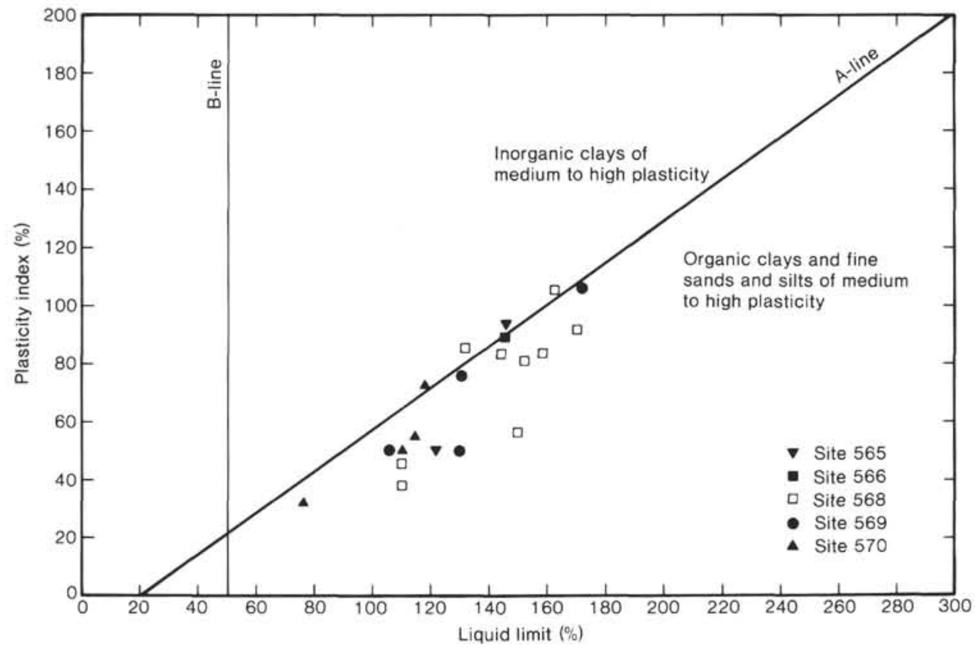

Figure 4. Atterberg limits and classification for Leg 84 sediments.

Table 1. Consolidation samples, Leg 84 drill sites.

Hole-Core-Sec.	Sub-bottom depth (m)	Water content (%)	Porosity (%)	Void ratio[a]	Bulk density (Mg/m^3)	Undrained shear strength (kPa)	Void ratio at P_C'	Compression index	Overburden pressure (kPa)	Preconsolidation pressure (kPa)	Overconsolidation ratio	Permeability (cm/s)
Site 565												
565-1-4	4.5	147	78	3.44	1.34	27	3.28	1.217	12	10	0.833	1.28E-5[b]
565-10-6	95.4	88	69	2.18	1.51	85	2.08	0.672	440	42	0.095	2.35E-7
Site 566												
566-1-2	2.8	85	66	2.27	1.49		1.94	0.961	10	400	38.952	4.30E-8
Site 568												
568-3-3	17.40	123	74	2.90	1.38	60	2.62	0.859	46	24	0.522	2.95E-8
568-6-2	50.90	77	64	2.52	1.56		2.23	0.739	170	33	0.194	7.70E-8
568-10-3	84.40	99	70	2.54	1.48	65	2.28	0.615	300	13	0.043	3.42E-7
568-12-3	102.10	88	69	2.39	1.49	161	2.17	0.595	380	30	0.079	2.39E-8
568-15-5	134.75	97	71	2.47	1.45	60	2.34	0.630	520	14	0.027	1.80E-7
568-18-4	162.25	104	73	2.85	1.44	125	2.46	0.800	610	40	0.066	2.55E-7
568-22-4	200.85	79	66	2.03	1.51		1.69	0.525	730	61	0.084	2.38E-7
568-25-4	230.35	112	73	3.06	1.42	105	2.45	1.100	860	180	0.209	1.60E-6
568-28-4	259.25	98	69	2.22	1.48	196	1.82	0.670	980	200	0.204	1.30E-7
568-29-4	268.95	85	68	2.28	1.53		1.92	0.650	1010	105	0.104	1.80E-7
Site 569												
569-2-3	5.55	102	71	2.47	1.43	180	2.22	0.837	23	47	2.043	1.21E-7
569-5-2	33.20	130	75	3.10	1.37	295	2.75	1.230	110	140	1.273	9.10E-8
569-8-2	61.80	76	66	2.11	1.52	250	1.86	0.835	205	160	0.780	1.35E-7
569-12-4	103.00	74	63	1.93	1.60	465	1.62	0.851	430	660	1.535	1.20E-7
Site 570												
570-1-2	3.0	91	70	2.18	1.50	210	1.97	0.566	11	19	1.727	9.50E-8
570-3-5	24.9	65	56	1.89	1.65	400	1.67	0.500	114	48	0.421	1.89E-7
570-6-5	53.7	73	63	1.76	1.54	284	1.53	0.523	150	115	0.767	4.50E-7
570-9-1	76.8	71	64	1.90	1.54	300	1.67	0.666	360	135	0.375	8.90E-8
570-14-1	125.0	75	64	1.88	1.56	545	1.63	0.786	600	350	0.583	1.87E-7

[a] Initial void ratio measured from consolidometer data with no load.
[b] 1.28E-5 = 1.28×10^{-5}.

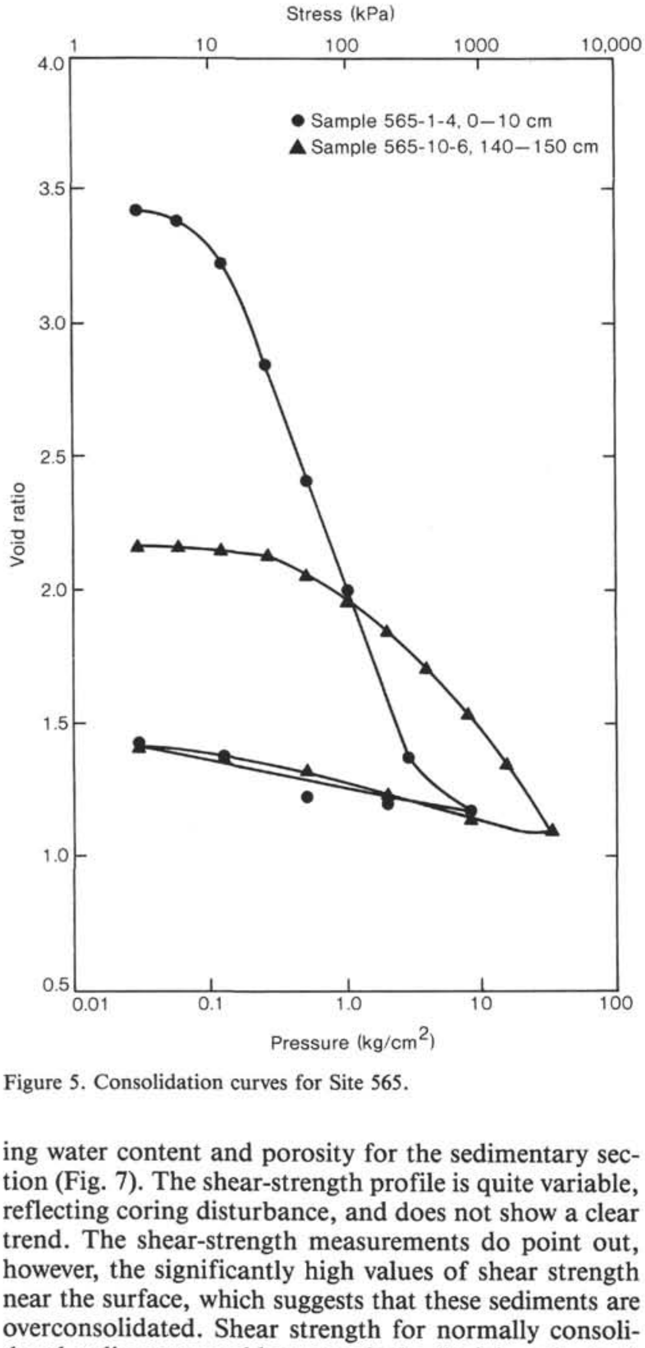

Figure 5. Consolidation curves for Site 565.

ing water content and porosity for the sedimentary section (Fig. 7). The shear-strength profile is quite variable, reflecting coring disturbance, and does not show a clear trend. The shear-strength measurements do point out, however, the significantly high values of shear strength near the surface, which suggests that these sediments are overconsolidated. Shear strength for normally consolidated sediments would approach the "origin cohesion" of approximately 1 to 5 kPa at the seafloor (Skempton, 1970), as opposed to values between 40 and 80 kPa.

One consolidation test was performed on sediments from this site, and the results of this test and permeability measurements are presented in Table 1 and Figure 8. The OCR (= 39) for this sample suggests that the sediment had equilibrated at some point to a greater overburden pressure, or that it has undergone cementation. The absence of cementation, as deduced from visual inspection of the sample, and the proximity of this site to a high-energy environment, such as is found along a submarine canyon wall, lead to the conclusion that erosive mechanisms have probably removed some overlying sediment. This is supported by paleontological evidence, since only Pleistocene and Miocene sediments were recovered. The curvature of the e-log P_0' curve does not show a well-defined break, and this suggests the possibility of some sample disturbance; but the OCR is sufficiently high as to indicate that this sediment has been preconsolidated. An effective vertical stress of 400 kPa (P_c') is comparable to the pressure created by approximately 90 m of slope sediment, as estimated from an average of all calculated relationships between vertical effective stress and sediment thickness for the Leg 84 Guatemalan margin sites. Thus, if the overconsolidation state observed at Site 566 is simply a problem of removed (eroded) overlying sediments, we can conclude that roughly 87 m of sediment have disappeared. Other mechanisms leading to overconsolidation include cementation, lateral (tectonic) stressing, and very slow sediment accumulation rates, but we find no evidence that these contributed significantly to the high OCR at this site.

A permeability of 4.3 10^{-8} cm/s, as measured on the consolidation sample, is within the expected values for the corresponding *in situ* void ratio (Table 1). Shipboard estimates of permeability, using a modified version of a falling-head permeameter, resulted in values comparable to the uncorrected (surface) value obtained for the consolidation sample. These two other estimates suggest that the permeability trend with depth is fairly constant within the sediment column, with values on the order of 10^{-8} cm/s, representing a nearly impermeable medium.

Site 567

This site is situated within the Middle America Trench slope (Fig. 6) in a 358-m-thick sedimentary section consisting of dark olive-gray muds and mudstones with numerous lithologic inclusions. The upper 200 m of the drilled section was washed, and the results, therefore, pertain only to the underlying sediments. The principal inclusions found consist of limestone, mudstone, and serpentinitic breccia. The results of grain-size analyses for three samples of the mudstone matrix are shown in Figure 9, and classify these sediments as clayey silts to silty clays. Carbonate content ranges from 3 to 15% for these three samples, and is composed principally of foraminiferal tests.

The index properties for this site strongly reflect the variable lithologies encountered, and present little information related to the character of the overlying sedimentary section (Fig. 9). Coring during Leg 67 at Site 494 recovered the upper sedimentary unit, and Atterberg limits for these sediments classify them as medium- to high-plasticity organic clays (Faas, 1982b). The sedimentary geotechnical section, as described by Faas (1982a), is one of rather quickly changing character to approximately 50 to 60 m sub-bottom, at which depths lithification of the mud into mudstone begins.

The consolidation behavior of the Site 494 sediment column, as presented by Faas (1982a), is one of normally consolidated sediments in the upper 46 m, changing to overconsolidated below 46 m. The overconsolidation is most likely a result of lithification and cementation. The C_u/P_0' ratio obtained from shipboard measurements of shear strength on Leg 67 yields an average value of 0.13

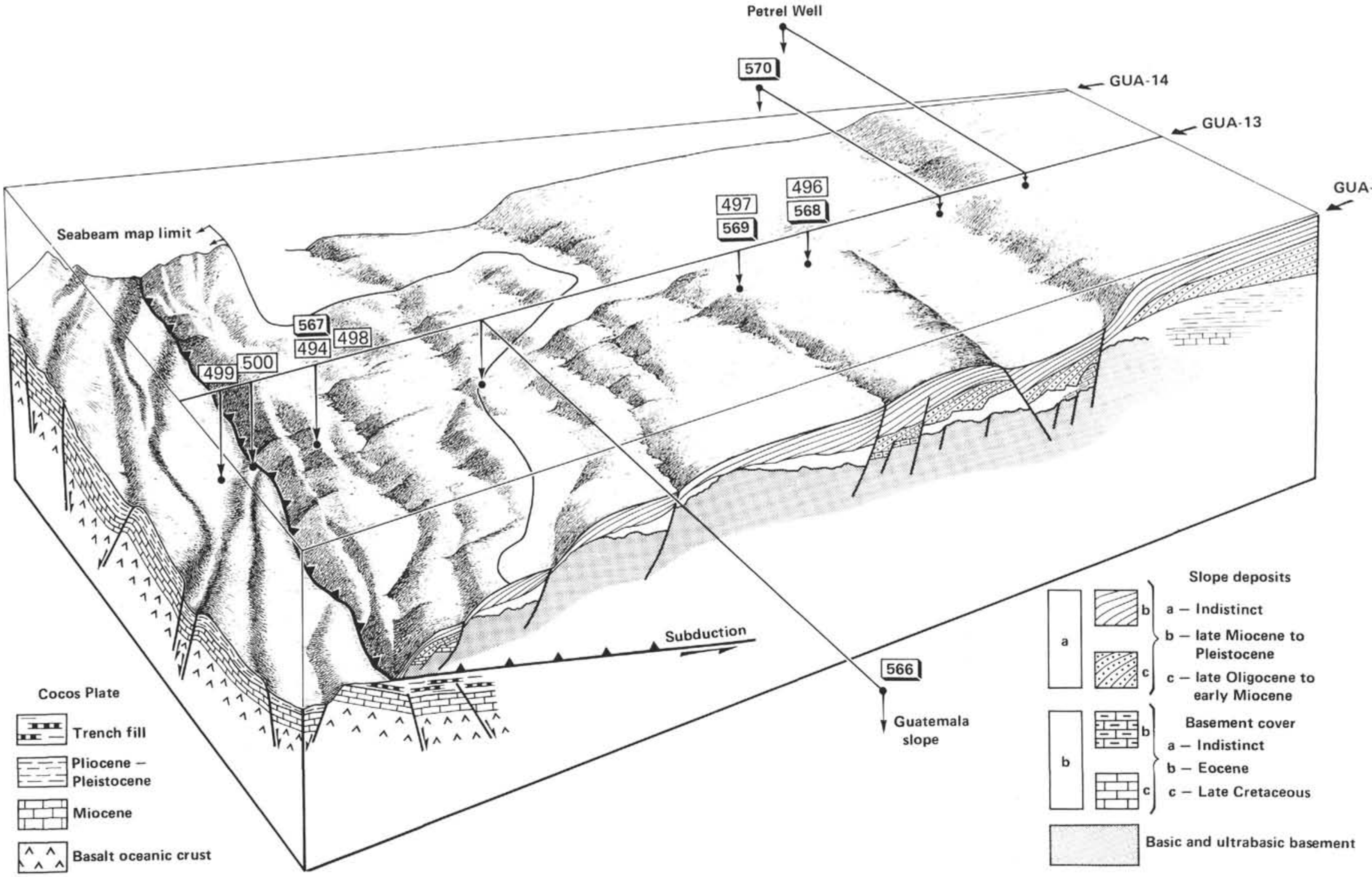

Figure 6. Perspective map showing Leg 84 study area off Guatemala and site locations along the Guatemalan margin.

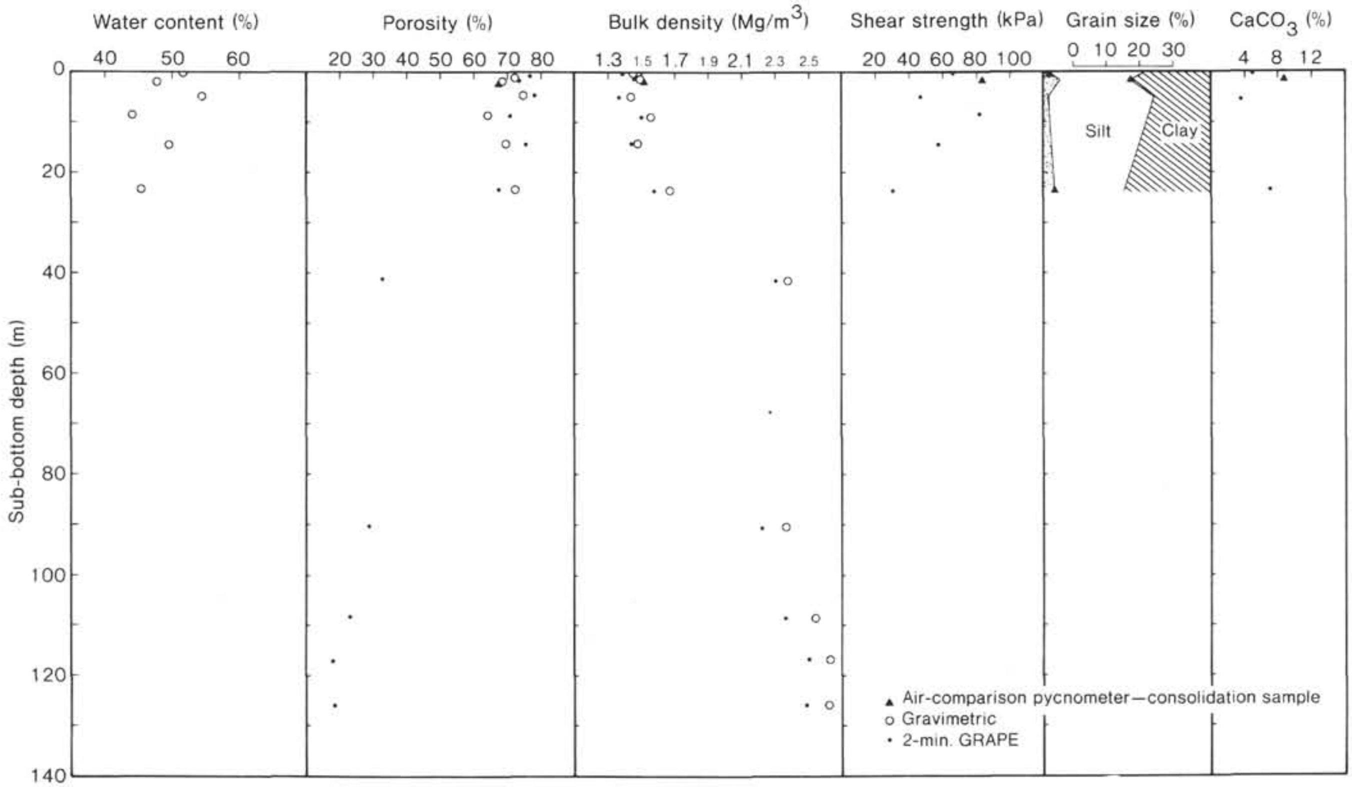

Figure 7. Geotechnical properties of sediments from Site 566.

for the upper 50 m, suggesting that this section may be underconsolidated. No consolidation tests were performed on Leg 84 samples, although two permeability measurements made on the ship resulted in permeabilities of 4.65×10^{-5} cm/s for Core 567A-2-4 and 1.58×10^{-6} cm/s for Core 567A-9-5. Correcting the surface permeability values to *in situ* conditions and assuming *in situ* porosities of approximately 60% would yield values of 10^{-7} to 10^{-8} cm/s, representing sediments of very low to practically no permeability.

Site 568

This site is on the upper slope of the Middle America Trench off Guatemala (Fig. 6). The upper part of the recovered sedimentary section consists of Recent to upper Pleistocene dark, olive-gray siliceous mud, which becomes partially lithified mudstone at approximately 180 m sub-bottom. Below this depth, the Pliocene–lower Miocene is a mud–mudstone sediment showing occasional unique fracture and deformation patterns described in detail by Cowan (1982) and Ogawa and Miyata (this volume). Grain-size analyses performed at the shore-based laboratory yield the profile in Figure 10, showing a predominantly silty clay with increased coarse material at depth, possibly resulting from incipient interparticulate cementation and lithification. Atterberg limits for sediments from this site classify them as medium- to high-plasticity organic clays or fine sands and silts (Fig. 4), concurring closely with the results for Leg 67 Site 496, only 1.5 km away (Faas, 1982b).

Bulk densities increase gradually from surface lows of 1.31 Mg/m^3 to 1.45 Mg/m^3 at 230 m. The Pleistocene/Pliocene boundary is marked by a more rapid increase in the bulk-density profile at 230–240 m sub-bottom, below which the gradient in index properties is similar to that in the upper section. A similar break in the gentle gradient of physical properties, at 360 to 375 m, may be related to a lower/middle Miocene boundary or hiatus.

The shear-strength profile for this site is quite disrupted, owing to significant degassing of the sediments upon retrieval (Fig. 10). Expansion of interstitial gas breaks down the bonding present between particles, and increases the sample void volume. The maximum C_u/P_0' ratio for this site is approximately 0.18, which would normally suggest an underconsolidated state. These sediments, however, do not follow the relationship defined by Skempton (1970), since gas disruption of the section will produce decreased shear strengths. The general trend of average shear-strength values shown by Faas (1982a) results in a C_u/P_0' ratio of approximately 0.36, and would support the conclusion that this sediment forms a more normally consolidated section.

Ten consolidation tests were performed on samples from this site; results are summarized in Table 1 and Figures 11 through 13. The curvature of the e–log P_0' curves from recompression to the virgin curve suggests that these samples are disturbed to various degrees. The estimated OCR values clearly reflect the effects of degassing, producing what would generally be interpreted as an underconsolidated section. Factors that may lead to a state of

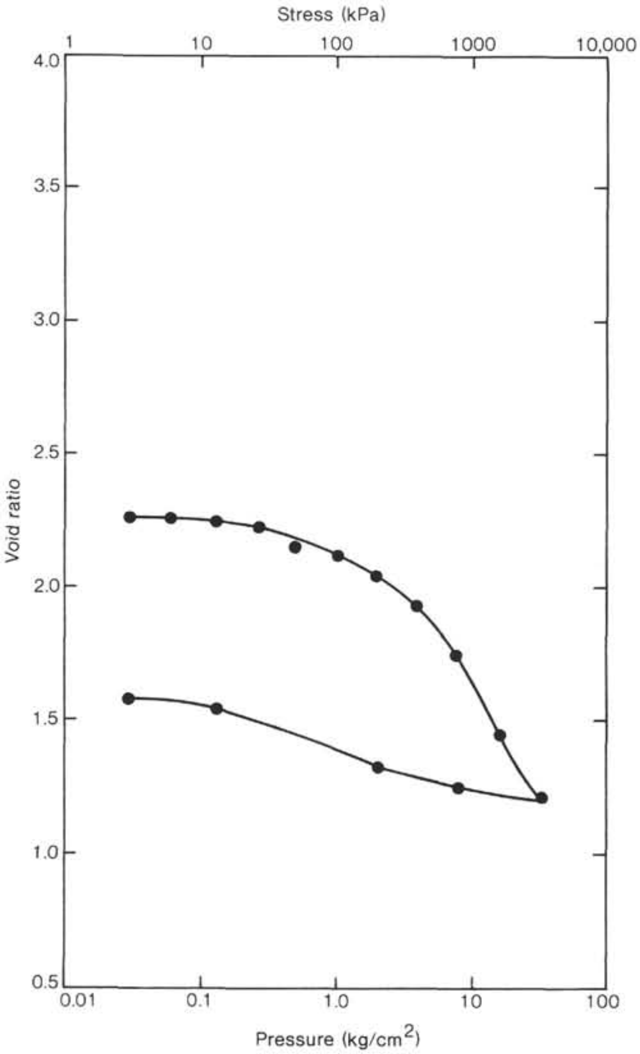

Figure 8. Consolidation curve for Site 566 (Sample 566-1-2, 130–135 cm).

underconsolidation include high sediment accumulation rates and high internal pore pressures. The latter agent may indeed be significant in the state of consolidation of sediments from Site 568, since excess downhole pressures were recorded during drilling. The presence of gas and dispersed hydrate found at this site can also contribute to this phenomenon.

Permeability measurements obtained in the laboratory show values ranging from 3.36×10^{-6} to 1.15×10^{-7} cm/s for *in situ* estimates. These values are interpolated at the predicted void ratio for P_o', but if the estimate for preconsolidation stress is low because of degassing effects on the consolidation results, the effective permeabilities could indeed be less. As it is, values of 10^{-6} to 10^{-7} cm/s represent very low degrees of permeability.

Site 569

Site 569 is on the mid-slope of the Middle America Trench off Guatemala (Fig. 6). The material recovered from 0 to 57 m consists of an upper, conformable sediment drape of dark olive-gray siliceous mud with interspersed ash layers. Below this zone is a 200-m-thick sequence of olive-gray to grayish blue-green mud and mudstone forming a prograding lobe, as interpreted from the geophysical record. The lowermost sedimentary section consists of a series of interbedded mudstones and calcareous mudstones. Laboratory grain-size analyses show that the uppermost unit is a silty clay, whereas the underlying prograding lobe unit contains a clayey silt in the uppermost part, grading to a silty clay downhole (Fig. 14). The Atterberg limits for these sediments, shown in Figure 4, classify them as having medium to high plasticity. A difference in the character of sediments is evident, considering that Atterberg limits of sediment belonging to the upper unit fall much closer to the A-line than those of the underlying unit.

The index properties for this site resemble those obtained for Site 568, showing a gradual gradient in all properties. Bulk densities, for instance, increase from subsurface values near 1.40 Mg/m^3 to 1.80 Mg/m^3 toward the bottom of the sedimentary section (Fig. 14). Deviations from the overall trend are noticeable at sub-bottom depths of 60 and 115 m, the uppermost representing the Pliocene/Miocene boundary.

The shear-strength profile also shows a very small increase in strength with depth, possibly reflecting to some degree the disturbance resulting from degassing. The maximum ratio of C_u/P_o' is approximately 0.21, which would indicate normally consolidated to slightly underconsolidated sediments relative to the average marine values reported by Skempton (1970).

Results of four consolidation tests on sediments from Site 569 are shown in Figures 15 and 16, and summarized in Table 1. The forms of the e-log P_o' curves suggest that the samples were relatively undisturbed, with the possible exception of Section 569-12-4. The OCRs for these samples show that states of overconsolidation occur at three intervals, whereas Section 569-8-2 is slightly underconsolidated. Compressional indices, C_c, for these sediments average 0.94, representing moderately compressible sediments.

Permeability results from laboratory and shipboard tests show little change with depth. Permeabilities range between 1.22×10^{-6} to 1.0×10^{-7} cm/s for interpolated *in situ* values. These permeabilities are consistent with similar values reported by Bryant et al. (1981) for silty clays and clayey silts at comparable void ratios.

Site 570

Site 570 is on the upper slope of the western Guatemalan margin (Fig. 6). Coring at this site recovered four sedimentary units overlying a serpentinized peridotite basement. The upper unit is 210 m thick and consists of olive-gray Pleistocene hemipelagic sediments with interspersed sand layers; lithification first appears at approximately 145 m sub-bottom. Below this unit is a 50-m-thick Pliocene mudstone also containing sand and occasional ash layers. The third unit is a lower to upper Miocene section of grayish olive mud, mudstone, and shale, and contains solid hydrate dispersed throughout. The final sedimentary unit consists of a series of interbedded muds, mudstones, limestones, and sands. The physical

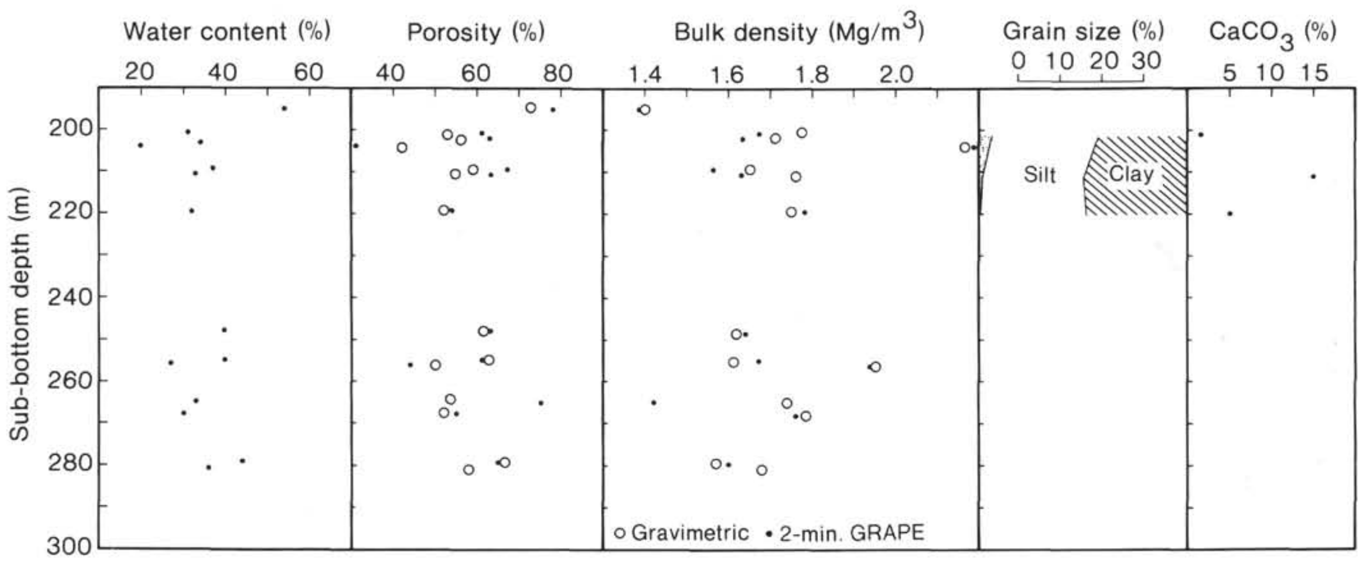

Figure 9. Geotechnical properties of sediments from Site 567.

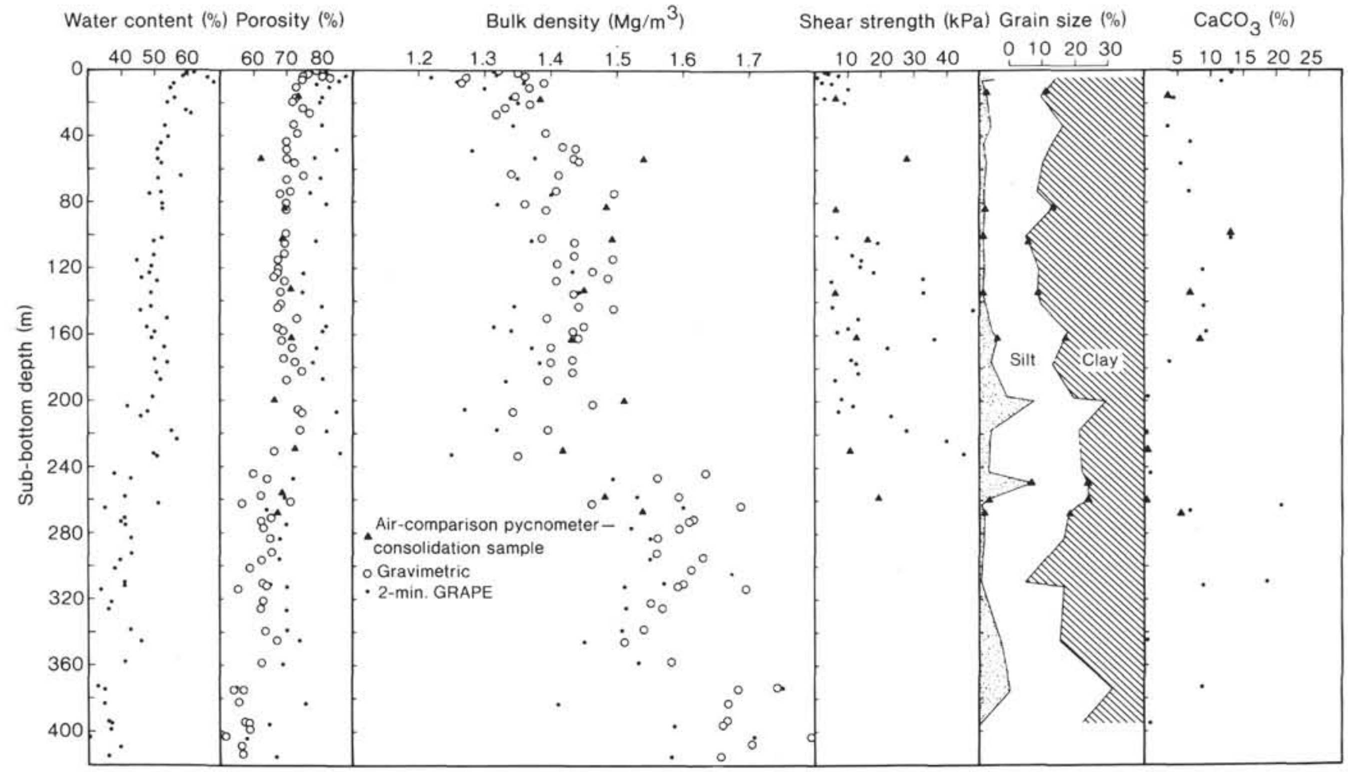

Figure 10. Geotechnical properties of sediments from Site 568.

properties of these different lithological types are quite distinctive, and are listed in the site chapter.

Grain-size analyses, plotted in Figure 17, characterize the sediments as silty clays to clayey silts with a few sandy horizons. The Atterberg limits obtained from trimmings of the consolidation samples yield the liquid limits and plasticity indices for these sediments, as plotted in Figure 4. These limits fall within the zone classified as fine sand and silts or organic clays of medium to high plasticity. Calcium carbonate content ranges from 4 to 27% in the samples tested, reflecting the variability of this component in the hemipelagic sequence.

Index properties at this site illustrate the typical geotechnical profile for marine sediments, showing a rapid change of properties near the sediment surface and becoming more gradual with increasing depth (Fig. 17). Water contents decrease from 52 to 43% in the upper 20 m, and then only shift from 43 to 40% at depths of approx-

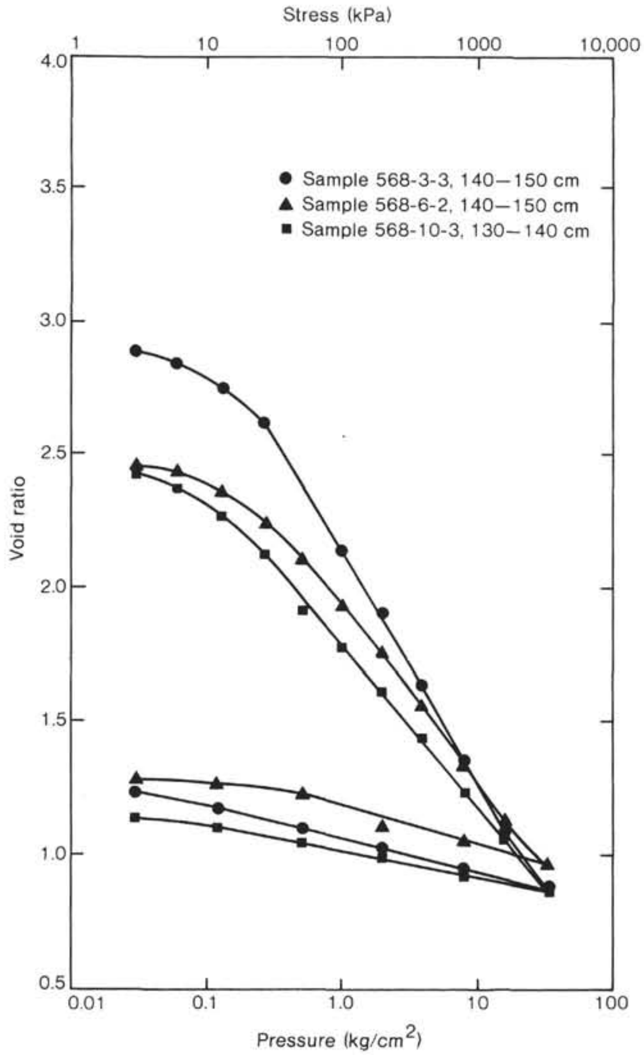

Figure 11. Consolidation curves for Site 568 sediments.

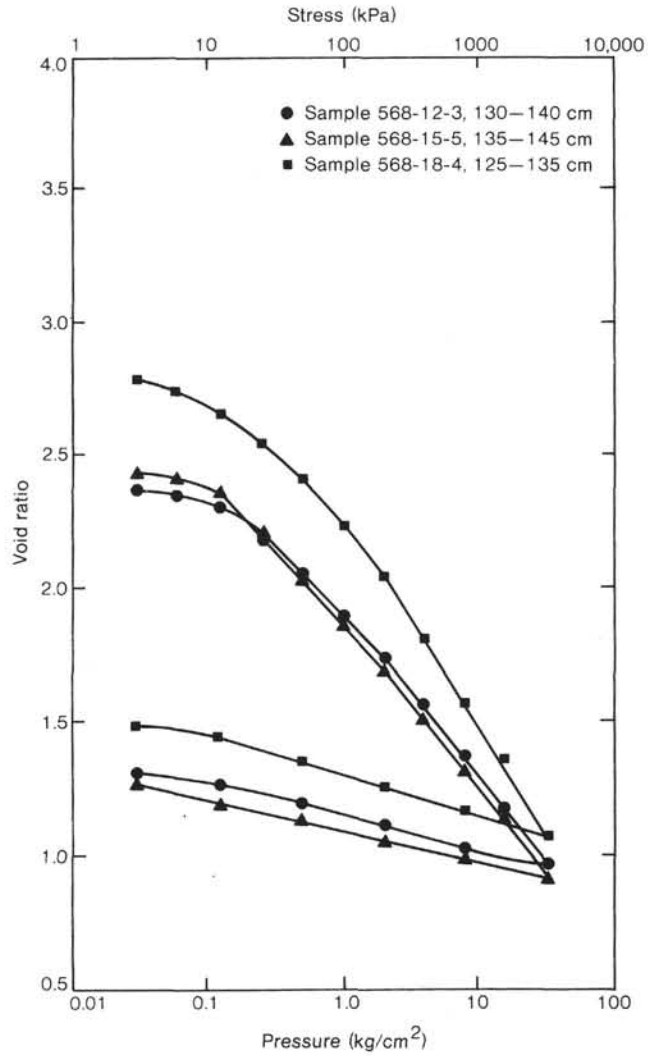

Figure 12. Consolidation curves for Site 568 sediments.

imately 200 m. The remaining section below 20 m is one of nearly constant values for the index properties, save the variable lithologic events recorded throughout the column.

The shear-strength profile (Fig. 17) shows a gradual increase in strength downhole, with some divergence at certain intervals, probably as a result of degassing. The estimated $C_u/P_0{}'$ ratio for the upper 100 m is 0.15, which represents an underconsolidated state for these sediments. This is comparable to results for the section at Site 568, and could be attributed to similar processes.

Five consolidation tests were performed on sediments from Site 570; results are shown in Figures 18 and 19 and summarized in Table 1. The curvature of the reload portion of the curve to the virgin curve in these figures reflects the fact that some disturbance may have occurred in samples from Sections 570-3-5 and 570-6-5. In general, however, the curves are consistent and OCR ratios are less than 1. These overconsolidation ratios suggest a degree of underconsolidation, as does the $C_u/P_0{}'$ ratio. The sample from Section 565-1-2 is overconsolidated, but it is not uncommon to find sediments with OCR values in excess of 1 at very shallow depths. This apparent state arises from an internal strength of sediments denoted as "origin cohesion."

Permeabilities obtained from shore-based laboratory measurements substantiate shipboard falling-head tests for uncorrected surface values. The range of permeability interpolated for *in situ* void ratios lies between 1.22 $\times 10^{-6}$ and 1.22 $\times 10^{-7}$ cm/s. These would be considered to represent sediments with a very low permeability.

DISCUSSION

Consolidation

Gravitational consolidation is the process by which the void space within a given sediment is decreased, resulting in closer arrangement of particles, and it is recognized generally by increased shear strengths and bulk densities and decreased water contents and porosities. The mechanism driving gravitational consolidation is the weight of the overlying sediment or overburden. The theory of consolidation, as presented by Terzaghi (1941), describes the nature of sediment dewatering as it is related to the dissipation of excess pore pressures created

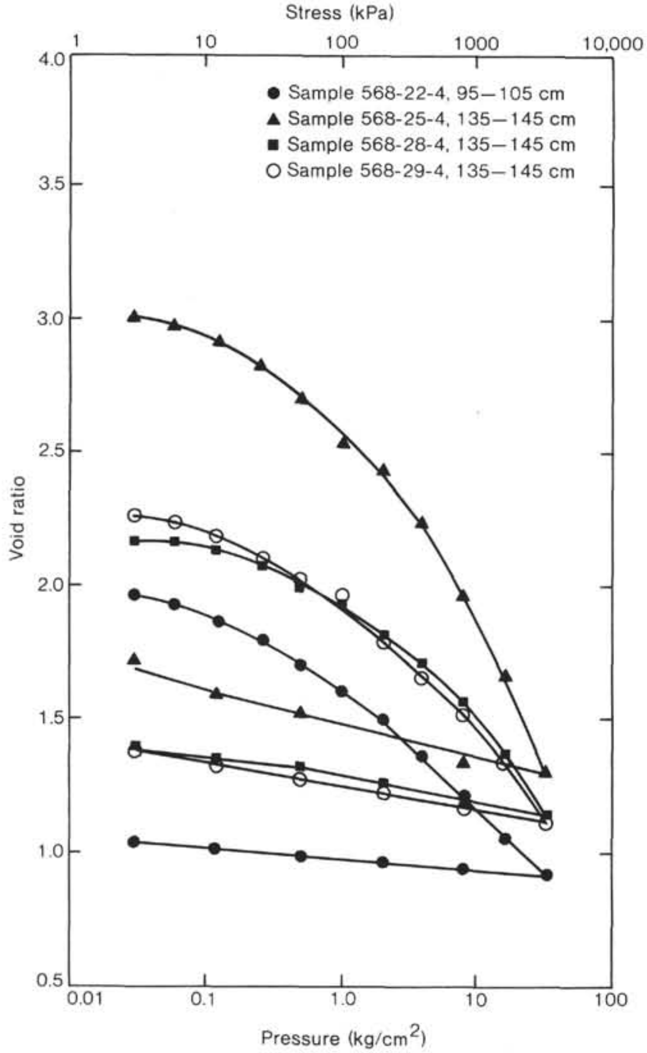

Figure 13. Consolidation curves for Site 568 sediments.

by the imposed overburden. Dissipation of these excess pore pressures allows the sediment to consolidate; lack of dissipation would result in an underconsolidation of the sediment. The underconsolidated state may also arise from rapid sediment mass accumulation rates, in which case dewatering of buried sediments and dissipation of the excess pore pressures is impeded by the rapidly imposing overlying material.

Sediments on the Middle America Trench slope contain significant amounts of gas, both in solution and as dispersed and massive hydrate. The production of gas within a saturated sediment causes another phase to attempt to occupy a given volume within the sediment pore space, and this leads to excess pore pressure if drainage is limited. This increased pore pressure, in turn, may impede the natural consolidation process, resulting in underconsolidated sediments such as those described for Sites 565, 567, 568, and most of 570. The observed degree of underconsolidation may be augmented by the disturbance created by gas expansion when the cores are retrieved, resulting in the poorly defined break of e–log P_0' curves and limiting our ability to draw conclusions as to the consolidation character of the sediments.

Downhole pore-pressure probe tests at Site 568 revealed apparent excess pore pressures on the order of 1020 kPa (150 psi) at 89.4 and 137.2 m sub-bottom, 1360 kPa (200 psi) at 186.2 m, and 2040 kPa (300 psi) at 360 m sub-bottom. Downhole excess pore pressures were also evident in Hole 567A when the bit became stuck downhole; the excess pore pressures in that hole were estimated to be on the order of 3400 kPa (500 psi) at a depth of 500 m (see Site 567 chapter). Pore pressures above hydrostatic pressure were also observed at the base of Hole 569 and possibly in Hole 565. The factors leading to excess pore pressures and resultant underconsolidated sediments include the following:

1. The presence of gas and decomposition of gas hydrates.

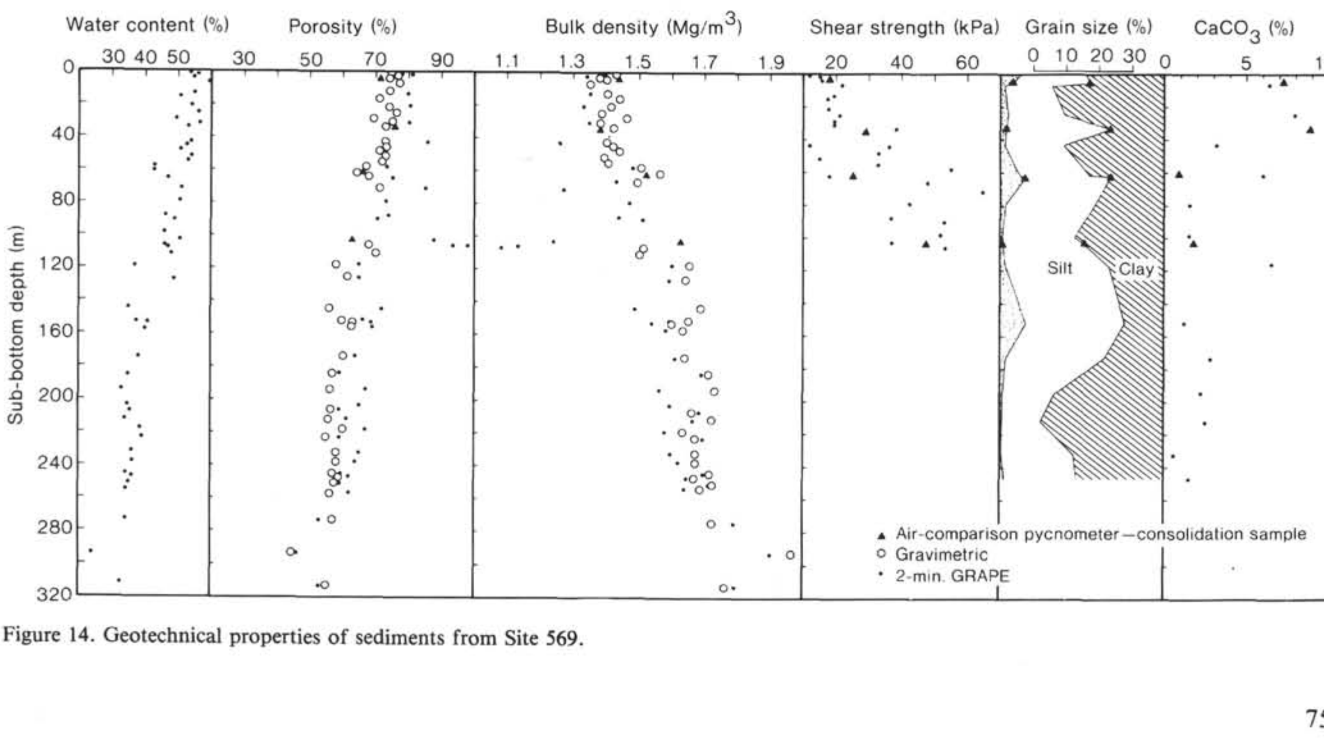

Figure 14. Geotechnical properties of sediments from Site 569.

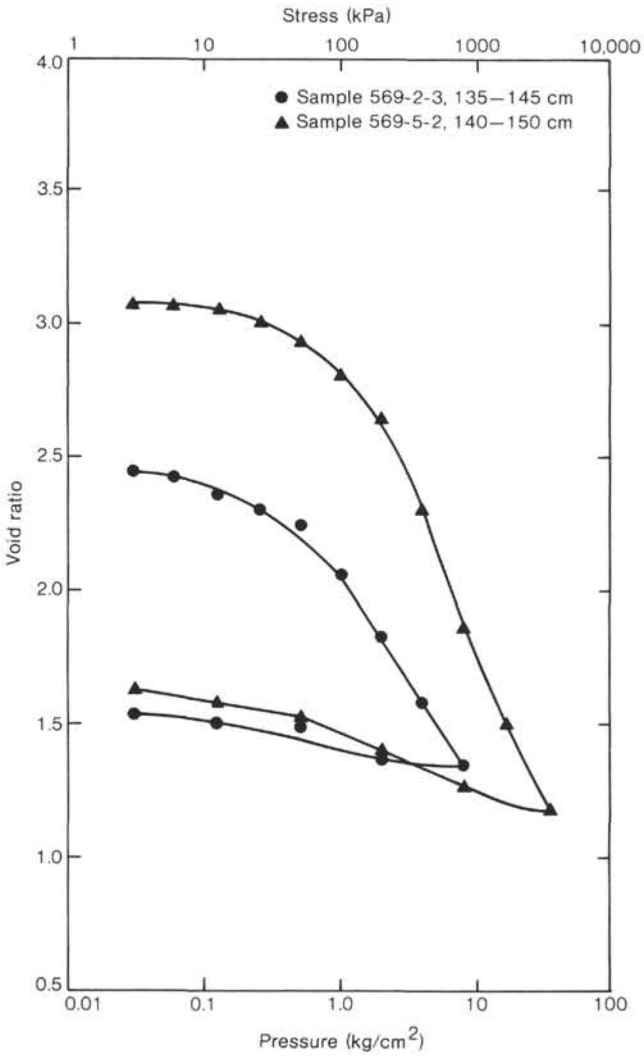

Figure 15. Consolidation curves for Site 569.

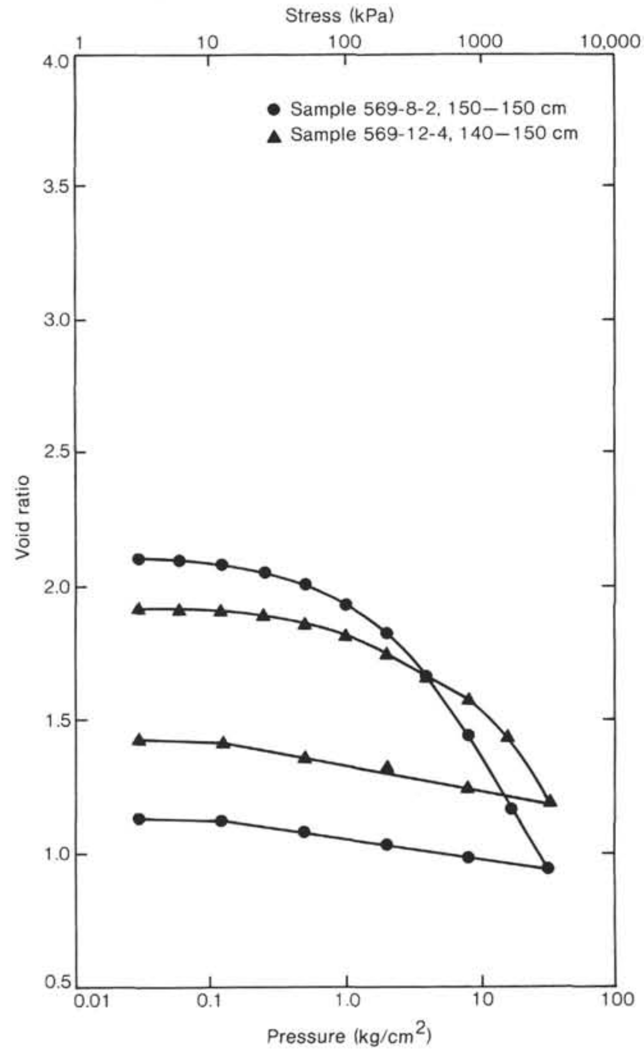

Figure 16. Consolidation curves for Site 569.

2. Abrupt local loading or very rapid rate of sediment accumulation.

3. Injection of pore fluids derived from the burial of oceanic and slope sediments under the overlying trench slope complex during the subduction process (Aubouin et al., 1982).

The subduction process would create an increasingly larger overburden on the subducted sediment unit, and any consolidation would result in expulsion of pore water into adjacent sediments and fractures. It is also evident that such an injection of excess fluid into the overlying sediments of the Middle America slope would lead to inhibition of the natural consolidation process and would be capable of producing the observed underconsolidated sections.

Sediments can reach the contrasting state of overconsolidation through a combination of mechanisms that may include (1) incipient cementation, (2) very slow rates of sediment accumulation and aging, (3) tectonic stressing, and (4) erosion of overburden. Site 566 presents a perfect case of removed overburden. A sediment column at this site in the San José Canyon is exposed to processes ranging from down-canyon current scour that would inhibit sediment accumulation to slope instabilities capable of eroding significant volumes of previously deposited material. The variable sediment thickness required to produce the excess overburden observed at Site 566 can be calculated from data for other Leg 84 slope sites (Figure 20). From these calculations an average sediment thickness of 87 m is required to provide the measured vertical effective stress. The estimated 87 m of removed overburden is also a conservative estimate if we consider that most sedimentary sections sampled along this trench slope are not normally consolidated, but underconsolidated.

Site 569 exemplifies a somewhat overconsolidated section, regardless of the excess pore pressures registered during drilling operations. This contradicts the consolidation state suggested by the C_u/P_o' ratio for this site and by Faas's (1982a) data for Site 497. Very slow sediment accumulation rates do not appear to have been significant contributors to the state of overconsolidation observed at Site 569, nor does tectonic stressing seem to have been an agent, since the sedimentary structures

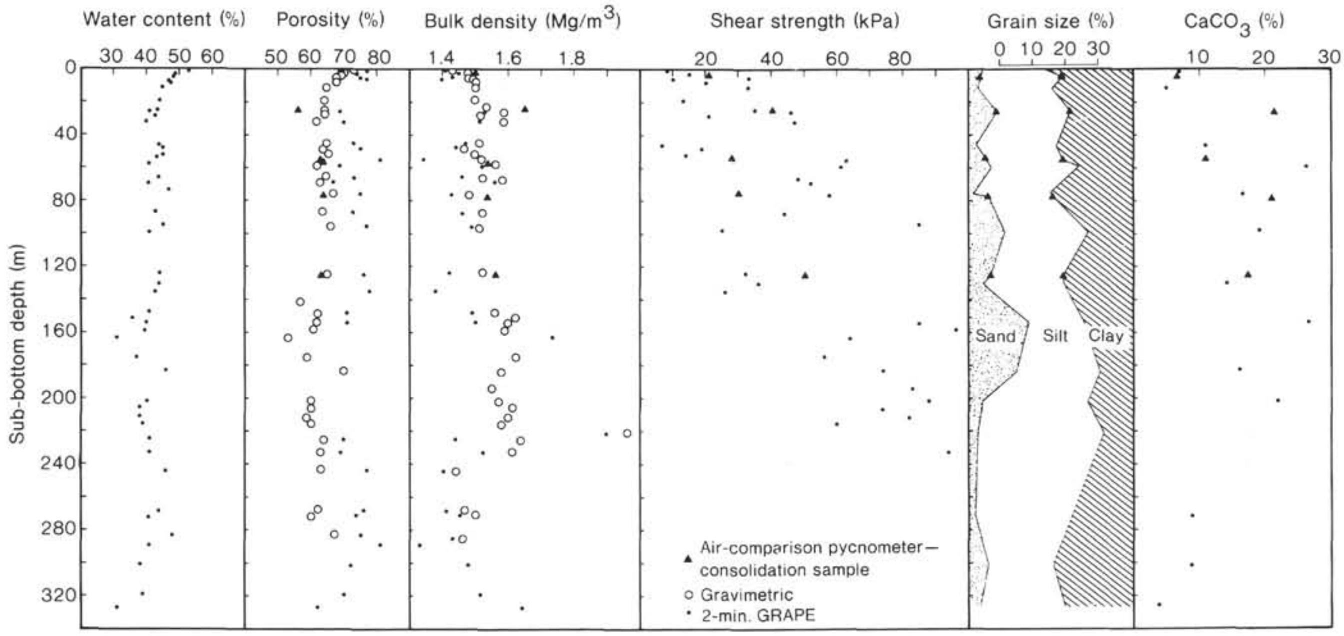

Figure 17. Geotechnical properties of sediments from Site 570.

show no evidence of folding or faulting. The most plausible explanations are initial cementation, local stressing, or erosional episodes resulting from a mass depositional process. Cementation and the formation of mudstone are not recorded in the section at Site 569 above depths of approximately 100 m, so it is conceivable to envision some episodes of erosion (possibly linked to observed biostratigraphic hiatuses), combined with slope sedimentation processes involving downslope creep and mass-movement events. These latter events can alter the geotechnical nature of the deposit, depending on the mechanism actively emplacing the unit. Booth (1979) describes the nature of overconsolidated sediments as they are related to different downslope transport mechanisms, and describes the gradually to abruptly overconsolidated state of a sedimentary unit as a recognizable attribute of flow deposits (e.g., debris and/or turbidity).

Permeability

Permeability and consolidation are two interdependent properties of a sediment, the rate of consolidation being controlled by how fast the water can dissipate under imposed excess pore pressures. Permeability is in turn related to the amount and size of interconnected voids within the sediment, which are constantly decreasing as the sediment consolidates. The general permeability trend for oceanic sediments of different grain-size characteristics is presented by Bryant et al. (1981). The permeability characteristics of the silty clays these authors describe are closely mimicked by the Leg 84 data. The overall trend of Leg 84 permeabilities can be seen in Figure 21.

The presence of excess pore pressures monitored at Sites 565, 568, and 569 may indicate flow conditions restrictive of dewatering in these areas. Regardless of the cause of such excess pore pressure, the permeability of the overlying unit is insufficient to allow this pressure to dissipate. The data shown in Table 2 represent the average values of index properties at sub-bottom depths near 250 m. The porosity of sediments at that depth, usually mud or mudstone, is between 57 and 64%, and the corresponding average permeabilities range from 2×10^{-9} to 5×10^{-8} cm/s, respectively. The range of permeability described by Terzaghi and Peck (1967) for practically impermeable sediments is less than 10^{-7} cm/s. These low permeabilities obviously constrain the consolidation process severely, and can lead to increased pore pressures above hydrostatic conditions. The increasing mudstone component with depth at these sites reduces even more the effective permeability of the sediment, and may be the cause for restricted flow, leading to abnormal downhole pressures. The unique geochemical environment of the Guatemalan slope sediments, which contain abundant gas and hydrates, may also be an important determinant of permeability and flow conditions. The degree of saturation of a sediment is quite important to permeability. The greater the degree of saturation, the larger the permeability; thus, if these sediments contain a hydrate seal or a sufficient amount of gas not in solution and filling void spaces within the sediment fabric, we can expect a significant blockage of flow through these horizons.

Alternate flowpaths for fluid migration are along fracture planes, sandy-silt horizons, ash layers, and also perhaps through conduits evidenced in the unique vein structure described by Ogawa and Miyata (this volume) and by Cowan (1982). These flow paths correspond to the formation permeability, which may indeed be a very important consideration in the hydraulic history of this margin, but which unfortunately cannot be measured with the equipment or tests available. Interestingly, the availability of sand or silt horizons may be limited, since the general sedimentation pattern along this margin is one of

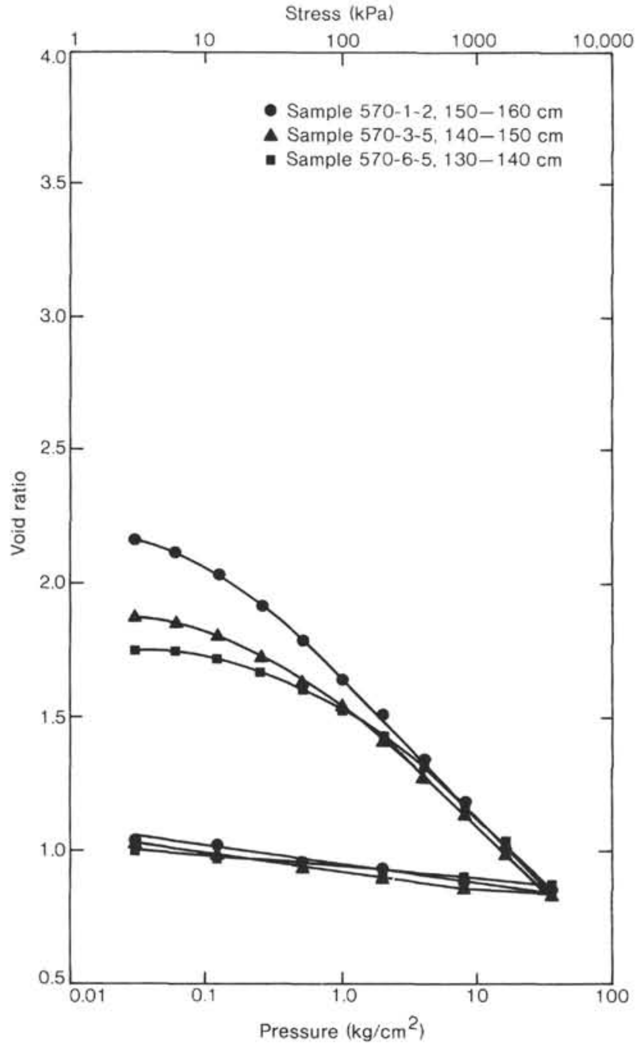

Figure 18. Consolidation curves for Site 570 sediments.

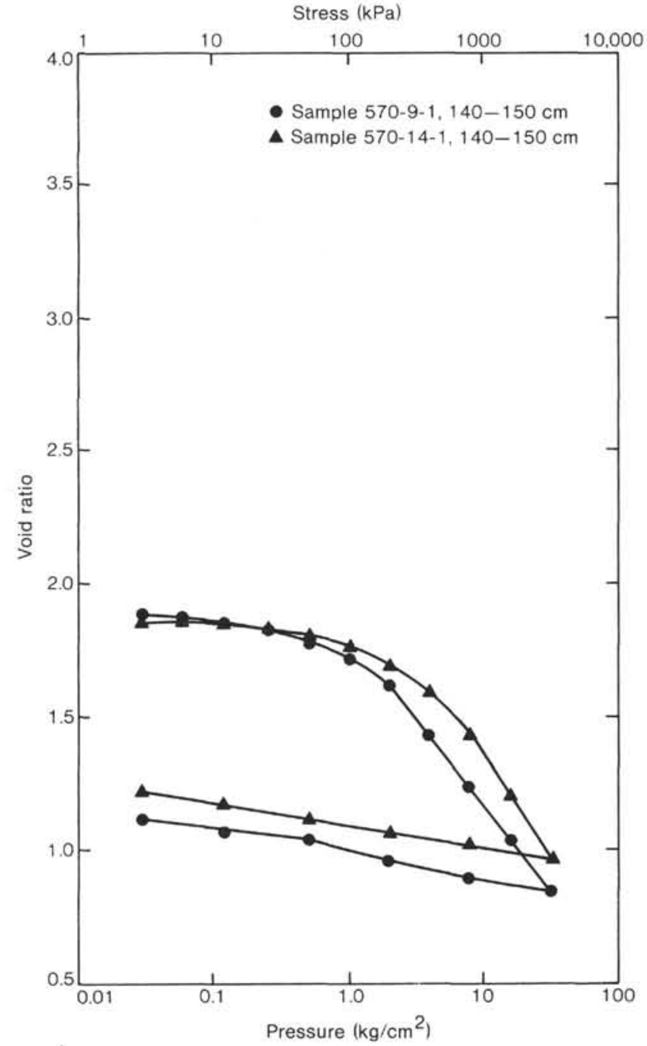

Figure 19. Consolidation curves for Site 570 sediments.

basin infilling. This generally results in only isolated cases of continuity regarding these horizons, thus limiting the effective lateral drainage of these more permeable layers. Added to the limited horizontal extent of these layers is the fact that massive hydrates were nearly always recovered within the coarser-textured sediments; this further limits the potential of these particular horizons to form high-permeability paths.

SUMMARY

The Middle America Trench slope sediments off Costa Rica and Guatemala have geotechnical characteristics consistent with hemipelagic, oceanic sediments from other portions of the world. Comparison of porosity-vs.-depth and permeability-vs.-depth relationships, for Leg 84 sediments, with the same relationships for sediments described by Bryant et al. (1981) shows that the slope deposits follow trends described for silty clay and clayey silts having 5–20% calcium carbonate. The disturbance created by degassing affects the consolidation state of sediments for at least three sites of Leg 84 and two others of Leg 67 (Faas, 1982a). Evidence of sediment erosion is strongly supported by the overconsolidated states of sediments at Site 566, and downslope transport mechanisms may be creating instances of overconsolidation at Sites 565 and 569.

Excess pore pressures present along this margin may be expected as a result of the presence of gas, of gas hydrate decomposition, of local downslope stressing, and of tectonically injected pore fluids resulting from the subduction of thick sediment piles. The occurrence and maintenance of these excess pressures, even with the appar-

Table 2. Summary of index properties for Middle America slope sediments at depths below 200 m sub-bottom.

Site	Sub-bottom depth interval (m)	Bulk density (Mg/m^3)	Porosity (%)	Water content (%)
565	220–240	1.66	58	37
567	220–240	1.70	57	35
568	270–290	1.57	64	42
569	222–240	1.65	57	35
570	220–240	1.62	63	40

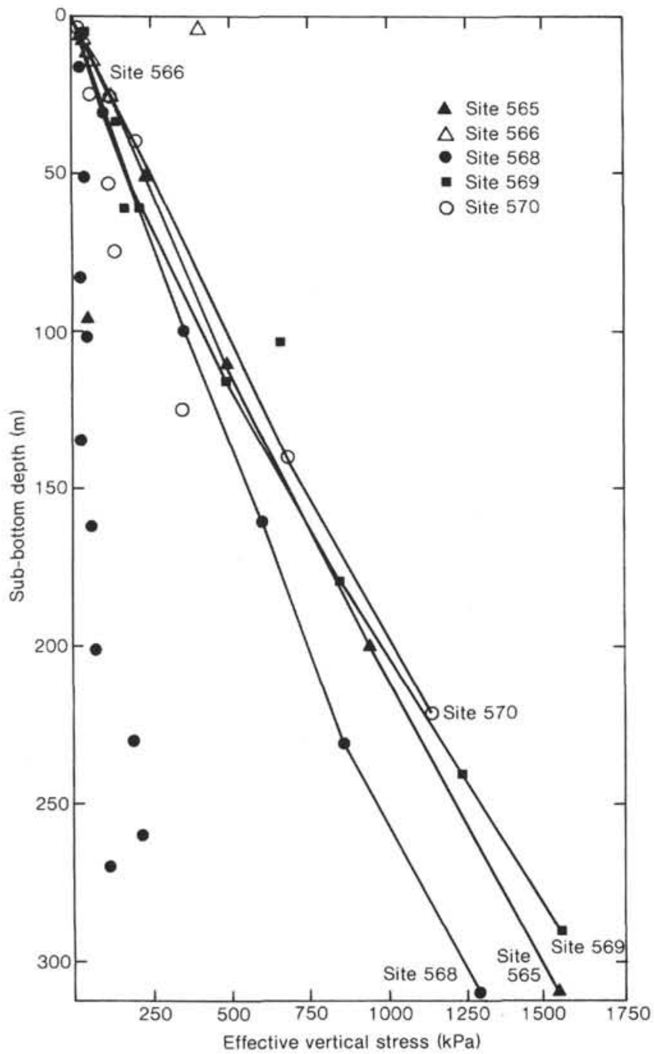

Figure 20. Profiles of *in situ* overburden and preconsolidated pressure vs. depth. Sediments corresponding to points on the *in situ* curves are normally consolidated, those above are overconsolidated, and those below the *in situ* profile are underconsolidated. The overburden corresponding to the equivalent thickness of a sediment column may be estimated from this figure.

ently fractured nature of mudstones and the presence of vein dewatering paths, support the idea of a widespread mechanism generating these excess pore pressures.

ACKNOWLEDGMENTS

We thank Dr. G. Keller for reviewing this manuscript and providing us with excellent suggestions toward improving it. We also extend our gratitude to all shipboard personnel of Leg 84 who made this cruise an enjoyable working experience.

REFERENCES

Aubouin, J., von Huene, R., and Scientific Party, 1982. Leg 84 of the Deep Sea Drilling Project, subduction without accretion: Middle America Trench off Guatemala. *Nature*, 297:458–460.

Booth, J. S., 1979. Recent history of mass-wasting on the upper continental slope, northern Gulf of Mexico, as interpreted from the consolidation states of the sediment. *Soc. Econ. Paleontol. Mineral. Spec. Publ.*, 27:153–164.

Bouma, A. H., 1969. Methods for the study of sedimentary structures: New York (Wiley Interscience).

Boyce, R. E., 1976. Definitions and laboratory techniques of compressional sound velocity parameters and wet-water content, wet bulk density, and porosity parameters by gravimetric and gravimetric and gamma ray attenuation techniques. *In* Schlanger, S. O., Jackson, E. D., et al., *Init. Repts. DSDP*, 33: Washington (U.S. Govt. Printing Office), 931–951.

Bryant, W. R., Bennett, R. H., and Katherman, C. F., 1981. Shear strength, consolidation, porosity, and permeability of oceanic sediments. *In* Emiliani, C. (Ed.), *The Sea*, (Vol. 7): New York (John Wiley & Sons), 1555–1615.

Casagrande, A., 1936. The determination of the preconsolidation load and its practical significance. *Proc. Third Int. Conf. Soil Mech. Found. Eng.*, pp. 60–64.

Cowan, D. S., 1982. Origin of "vein structure" in slope sediments on the upper slope of the Middle America Trench off Guatemala. *In* Aubouin, J., von Huene, R., et al., *Init. Repts. DSDP*, 67: Washington (U.S. Govt. Printing Office), 645–650.

Faas, R. W., 1982a. Gravitational compaction patterns determined from sediment cores recovered during the Deep Sea Drilling Project Leg 67 Guatemalan transect: continental slope, Middle America Trench, and Cocos Plate. *In* Aubouin, J. von Huene, R., et al., *Init. Repts. DSDP*, 67: Washington (U.S. Govt. Printing Office), 614–638.

________, 1982b. Plasticity characteristics of the Quaternary sediments of the Guatemalan continental slope, Middle America Trench and Cocos Plate—Leg 67, Deep Sea Drilling Project. *In* Aubouin, J., von Huene, R., et al., *Init. Repts. DSDP*, 67: Washington (U.S. Govt. Printing Office), 639–644.

Folk, R. L., 1974. *Petrology of Sedimentary Rocks*: Austin (Hemphill Publ. Co.).

Lambe, T. W., 1951. *Soil Testing for Engineers*: New York (John Wiley & Sons).

Lambe, T. W., and Whitman, R. V., 1969. *Soil Mechanics*: New York (John Wiley & Sons).

Lowe, J., Zaccheo, P. F., and Feldman, H. S., 1964. Consolidation testing with back pressure. *J. Soil Mech. and Found. Div., A.S.C.E.*, 90:69–86.

Shephard, L. E., 1981. Geotechnical properties of select convergent margin sediments [Ph.D. dissertation]. Texas A&M University, College Station, Texas.

Skempton, A. W., 1970. The consolidation of clays by gravitational compaction. *J. Geol. Soc. London*, 125:373–411.

Terzaghi, K., 1941. Undisturbed clay samples and undisturbed clays. *J. Boston Soc. Civil Eng.*, 28:211–231.

Terzaghi, K., and Peck, R. B., 1967. *Soil Mechanics in Engineering Practice* (2nd ed.): New York (John Wiley & Sons).

Date of Initial Receipt: 15 September 1983
Date of Acceptance: 6 February 1984

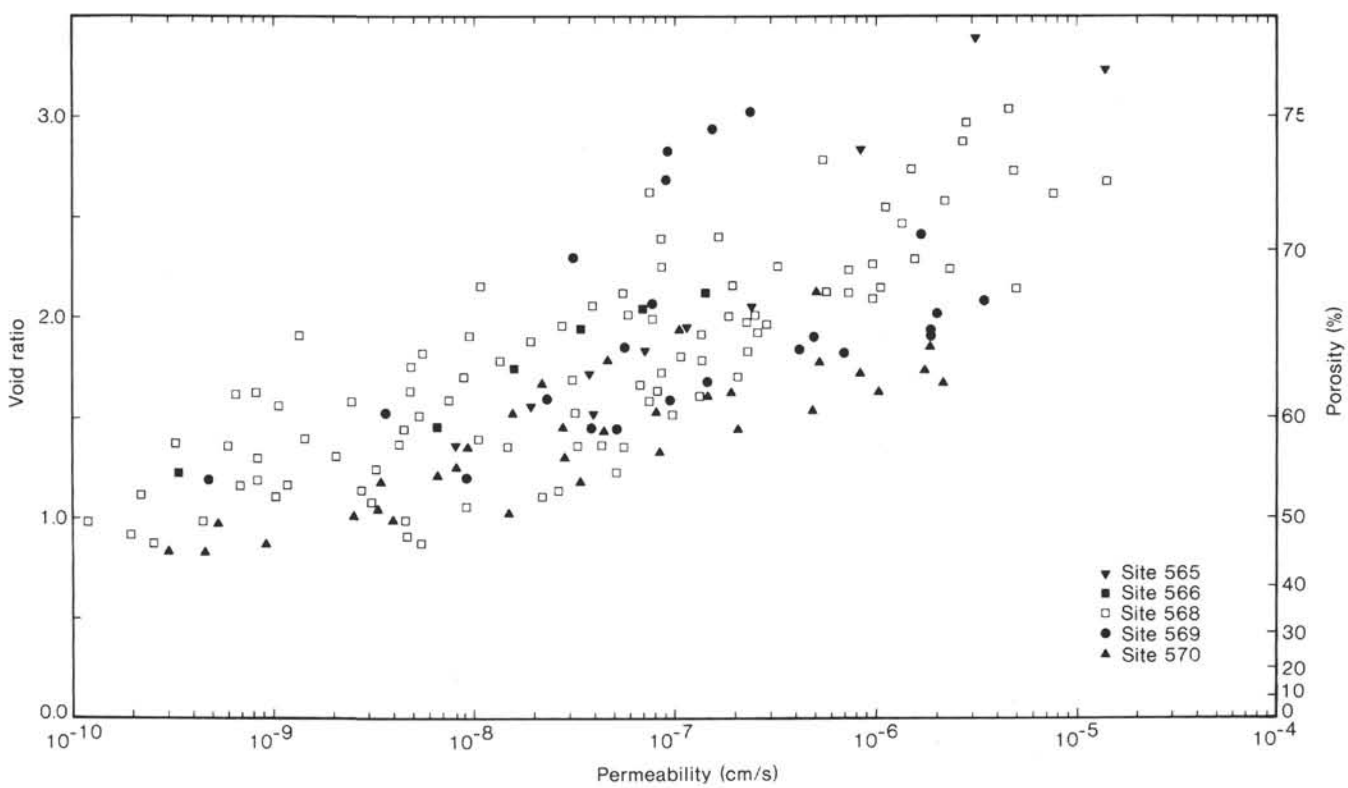

Figure 21. Permeabilities computed from consolidation tests at different void ratios for sediments from Leg 84.

APPENDIX
Geotechnical Summary, Leg 84

Core	Section	Sub-bottom depth (m)	Water content (%)	Porosity (%)	Bulk density (Mg/m^3)	Un-drained shear strength (kPa)	2-min. GRAPE porosity (%)	2-min. GRAPE bulk density (Mg/m^3)	Compressional-wave velocity (km/s)	Direction[a]
Site 565 (Hole 565)										
1	2	2.52	57			10	80	1.52	1.522	V
1	5	6.32	49			13	80	1.57	1.518	V
1	7	9.09	46			22	70	1.68	1.540	V
2	2	12.23	41			27	70	1.68	1.546	V
2	4	15.22	43			30	68	1.71	1.525	V
2	4	15.22							1.543	H
2	6	18.22	38			43	67	1.74	1.553	V
2	6	18.22							1.535	H
3	2	21.72	41			13	71	1.65	1.503	V
3	4	24.77	40			10	70	1.70	1.538	V
3	6	27.72	36			58	64	1.79	1.556	V
4	2	31.02	38			22	68	1.72	1.573	V
4	4	34.22	37			25	63	1.78	1.584	V
4	4	34.22						1.80	1.497	H
5	3	42.72	34			45		1.25	1.533	V
5	5	45.72	33			52	65	1.81	1.371	V
6	1	48.78	42			32	70	1.72	1.217	V
6	2	50.63	40				74	1.64	1.282	V
6	5	55.53	42			47	83	1.51		
7	2	59.83	38			68	79	1.60		
7	3	61.06	42			59	76		1.025	V
7	5	64.84	35			42				
8	3	71.41	42				71			
8	3	71.52	38					1.70	1.312	V
8	6	76.33	41			37	72	1.69		
8	6	76.33						1.65		
8	6	76.33						1.60		
9	3	81.18	37			23	78	1.57		
9	5	83.17	41			93	71	1.70	0.784	V
9	7	86.26	42			52	73	1.65		
10	1	87.93	40			26	71	1.71	0.803	V
10	5	93.13	39			17	74	1.71	1.551	V
10	5	93.13						1.65		
11	1	96.60	43				71	1.63	1.534	V
11	2	97.59	40			12	75	1.64	2.227	V
11	3	99.62	46			6	78	1.53	1.511	V
11	4	100.62	45			15	76	1.58	1.522	V
12	3	108.61	47							
12	5	112.12	49				73	1.60		
12	5	112.12						1.63		
12	6	113.67	45			16	63	1.76	1.567	V
13	2	116.75	42				71	1.61	1.561	V
13	4	119.82	39				66	1.68	1.177	V
13	6	122.88	44				71	1.61	1.523	V
14	2	126.17	42				70	1.63	1.584	V
14	4	129.16	40				65	1.69	1.532	V
14	6	132.23	37				65	1.70	1.592	V
15	2	135.68	47				77	1.58	1.575	V
15	4	138.68	42				76	1.63		
15	6	142.18					73	1.65		
16	1	143.59	33				71	1.70	1.574	V
16	3	147.84	33				71	1.71	1.063	V
16	6	151.42	32							
17	2	154.97	35				66	1.75	1.641	
17	4	157.65	33				72	1.66	1.571	V
17	6	160.99	33				70	1.71	1.687	H
18	1	162.78	34				72	1.70	1.589	H
18	3	166.35	35				69	1.75	1.610	V
18	4	168.28	31				73	1.68	1.638	V
19	1	172.51	31						1.847	V
19	3	175.01	32				66	1.80	1.105	V
19	6	180.71	31				68	1.78		
20	3	185.39	34				62	1.86	1.579	V
20	5	188.45	31						2.204	V
21	2	192.63	40				83	1.41		
21	4	196.73	40				70	1.62		
21	6	198.97	43				76	1.48	1.482	V
21	6	198.97						1.53		
22	4	206.14	35				66	1.76	1.608	V
23	1	211.08	30				59	1.90	1.638	V
23	6	218.49	37				65	1.80	1.620	V
24	2	222.05	33				68	1.75	1.630	V

Appendix. (Continued).

Core	Section	Sub-bottom depth (m)	Water content (%)	Porosity (%)	Bulk density (Mg/m^3)	Un-drained shear strength (kPa)	2-min. GRAPE porosity (%)	2-min. GRAPE bulk density (Mg/m^3)	Compressional-wave velocity (km/s)	Direction[a]
(Hole 565 Cont.)										
24	4	225.46	34				64	1.81	1.670	V
25	1	230.24	34				66	1.77	1.560	V
25	1	230.24						1.83		
25	3	233.14	13				34	2.33	2.286	V
26	4	243.78	34				71	1.70	1.619	V
28	1	258.33	31				68	1.75	1.585	V
28	1	258.33							1.619	V
29	2	269.20	28				61	1.86	1.753	V
29	6	275.44	28				60	1.89	1.678	V
30	1	276.91	30				60	1.89		
30	4	282.21	28				70	1.72	1.742	V
30	6	284.83	29				68	1.76	1.663	V
31	3	290.14	32				72	1.70	1.596	V
31	5	292.60	29				63	1.83	1.634	V
31	7	295.10	31				63	1.83	1.670	V
32	1	300.70					64	1.81	1.662	V
33	1	310.00					65	1.76		V
33	CC	311.80					67	1.71		
Site 566 (Hole 566)										
1	1	0.53	50	72	1.44	65	78	1.55	1.531	V
1	3	3.53	46	68	1.49	83	74	1.61	1.559	V
2	2	6.33	52	75	1.43	47	79	1.53	1.565	V
2	4	8.87	42	64	1.54	81	70	1.64		
4	2	14.83	48	70	1.46	58	75	1.54	1.558	V
5	2	24.35	44	73	1.66	31	67	1.66	1.588	V
7	1	41.49	6	14	2.37		32	2.52	3.901	
Hole 566C										
2	2	90.01	11	26	2.35		28	2.44	2.871	V
5	1	109.11			2.52		29	2.59	3.990	V
6	1	117.66			2.62		17	2.73	5.268	V
6	1	117.66							5.057	H
7	1	127.72			2.52		18	2.70	4.184	V
Site 567 (Hole 567A)										
1	4	201.19	30	53	1.77		61	1.86	1.605	V
1	6	203.35	33	56	1.71		63	1.83	1.678	V
1	6	203.72	19	42	2.17		31	2.40	2.031	V
2	3	209.58	36	59	1.65		67	1.75	1.528	V
2	3	209.58							1.590	V
2	4	210.96	31	55	1.76		63	1.83	1.536	V
3	4	219.80	30	53	1.75		54	1.99	1.764	V
6	4	248.38	38	62	1.62		63	1.82	1.687	V
7	2	254.65	38	61	1.61		61	1.88	1.763	V
7	2	255.15	26	51	1.94		44	2.14	1.802	V
8	2	264.95	31	55	1.74		75	1.63	1.778	V
8	3	266.96	29	52	1.78		55	1.96	1.775	V
9	4	277.38						1.76	1.704	V
9	5	278.88	42	66	1.57		65			
10	1	281.32	35	58	1.68				1.724	V
10	2	283.26	8	18	2.37		19	2.58	3.536	V
11	1	289.51			2.32		35	2.32	4.306	V
14	2	319.13			2.51		18	2.62	4.107	
16	1	334.20			2.33				2.670	V
16	2	336.12	23	42	1.87		51	2.06	1.902	V
17	1	343.80					24	2.52	3.179	V
17	3	346.35	21	40	1.93		45	2.16	1.748	V
19	1	359.42			2.35		20	2.60	2.884	V
20	1	377.62			2.69		5	2.81	4.820	V
21	CC	394.22			2.56				4.491	V
21	CC	394.22							4.586	H
25	1	429.60							4.244	V
25	1	430.00					4	2.72		
25	1	430.22	3	8	2.64		11	2.69	4.266	H
25	1	430.22						2.76	4.447	V
25	1	430.68					14	2.57		
25	2	431.15					11	2.62		
25	2	431.23					11	2.62	3.427	V

Appendix. (Continued).

Core	Section	Sub-bottom depth (m)	Water content (%)	Porosity (%)	Bulk density (Mg/m^3)	Un-drained shear strength (kPa)	2-min. GRAPE porosity (%)	2-min. GRAPE bulk density (Mg/m^3)	Compressional-wave velocity (km/s)	Direction[a]
(Hole 576A Cont.)										
25	2	431.63					12	2.61	3.213	V
25	2	431.72					20	2.46	3.427	V
25	2	432.26					12	2.64		
25	3	432.62					17	2.57		
26	1	438.55					7	2.72	4.247	V
26	1	439.60					10	2.73	4.261	V
27	1	446.87					8	2.68		
27	1	447.15					15	2.59		
28	1	465.66					16	2.63		
28	1	466.35					18	2.55	3.724	V
29	1	486.05						2.89		
29	2	486.27					21	2.79	4.594	V
29	2	486.91					16	2.49		
29	2	487.27					9	2.53		
29	2	487.37					11	2.51	3.833	V
29	2	487.50					7	2.56		
Site 568 (Hole 568)										
1	1	1.12	60	79	1.32	3	82	1.51	1.560	V
1	2	2.27	57	77	1.35	4	82	1.52	1.545	V
1	3	3.25	55	75	1.36	7			1.568	V
2	1	3.91	64	81	1.27	1	88	1.42	1.563	V
2	3	6.92	66	82	1.26	2	86	1.46	1.559	V
2	3	7.72	54	75	1.39	5	79	1.56	1.572	V
2	6	11.42	53	73	1.37	10	83	1.50	1.555	V
3	3	17.02	55	73	1.34	3	81	1.54	1.530	V
3	5	20.02	52	72	1.37	9	80	1.55	1.598	V
4	2	24.47	57	75	1.33				1.579	V
4	4	27.26	58	77	1.32				1.554	V
5	2	34.23	51	72	1.41		81	1.53	1.686	V
5	6	39.87	52	73	1.39				1.580	V
6	2	44.10	50	70	1.42				1.596	V
6	5	48.62	49	70	1.43		85	1.47		
7	2	54.04	49	70	1.43		79	1.57	1.596	V
7	4	56.17	50	72	1.44				1.680	V
8	2	64.05	56	75	1.34				1.565	V
8	4	66.05	50	71	1.42		80	1.56	1.614	V
9	3	73.86	51	71	1.41				1.550	V
9	4	75.76	45	67	1.49		77	1.60	1.578	V
10	2	81.82	52	70	1.36		82	1.50	1.800	V
10	4	84.78	51	70	1.39				1.708	V
12	2	101.01	50	70	1.38	7			1.243	V
12	4	104.09	48	68	1.43	19	79	1.55	1.166	V
13	3	112.01	49	69	1.43	11				
13	5	114.93	43	65	1.49	13				
14	2	119.73	48	67	1.41	13				
14	4	122.73	46	67	1.46	18	75	1.59		
14	6	126.14	45	66	1.48	33				
15	1	127.83	49	69	1.41	5			1.117	V
15	6	135.34	47	68	1.44	33	75	1.57		
16	4	142.53	47	68	1.44		81	1.53		
16	6	144.73	45	67	1.49	48				
17	3	150.23	52	73	1.39	13			1.703	V
17	6	155.63	46	67	1.45	10	82	1.49		
18	1	157.23	48	69	1.43	7	81	1.50		
18	4	161.63	48	69	1.44	36				
19	2	168.03	52	72	1.40	22	79	1.54		
19	6	175.03	48	69	1.43	11				
20	1	176.71	52	73	1.39	12	78	1.55		
20	6	183.88	49	71	1.43	13			1.579	V
20	6	183.88							1.524	V
21	2	188.44				8	81	1.53		
22	2	198.11	50						1.613	V
22	6	203.07				11	73	1.66	1.698	V
23	1	206.31	56	75	1.34	7	85	1.46	1.490	V
24	2	217.72	53	74	1.39	28	82	1.51	1.538	V
24	6	223.57	57			40				
25	5	231.76	49	66	1.35	45	86	1.41		
25	6	233.07	51			78				
27	1	244.13	37	60	1.63				1.660	V
27	3	247.17	41	64	1.56		71	1.69	1.606	V

Appendix. (Continued).

Core	Section	Sub-bottom depth (m)	Water content (%)	Porosity (%)	Bulk density (Mg/m^3)	Undrained shear strength (kPa)	2-min. GRAPE porosity (%)	2-min. GRAPE bulk density (Mg/m^3)	Compressional-wave velocity (km/s)	Direction[a]
(Hole 568 Cont.)										
28	4	258.47	39	62	1.59		69	1.73	1.600	V
28	7	262.84	49	71	1.46				1.578	V
29	1	264.17	34	57	1.68		64	1.81	1.682	V
29	6	271.26	40	65	1.62				1.557	V
30	1	273.76	39	62	1.61				1.542	V
30	4	277.49	39	63	1.59		70	1.72	1.699	V
31	1	283.27	42	65	1.56		68	1.76	1.550	V
32	1	292.45	42	65	1.56				1.563	V
32	4	296.84	39	63	1.63		68	1.76	1.568	V
33	1	301.67	37	59	1.61				1.574	V
33	6	310.03	40	63	1.60		65	1.81	1.648	V
34	1	311.71	39	62	1.59		70	1.72	1.561	V
34	3	314.31	33	55	1.69				1.423	V
35	1	321.91	41	63	1.55				1.491	V
35	4	326.36	40	62	1.57		70	1.71	1.397	V
36	6	339.37	41	64	1.54		70	1.70	1.494	V
37	4	345.33	44	67	1.51		74	1.65	1.711	V
38	6	359.07	39	62	1.58		69	1.74	1.480	V
40	3	373.34	31	55	1.74		55	1.94	1.583	V
40	4	375.40	34	57	1.68				1.663	V
41	3	383.27	34	56	1.67		76	1.62	1.646	V
42	4	394.84	35	58	1.67				1.547	V
42	5	395.09	35	59	1.66		66	1.79	1.547	V
43	1	398.74	35	59	1.67				1.546	V
43	4	403.42	29	52	1.79		58	1.92	1.709	V
44	2	409.91	33	57	1.71				1.566	V
44	5	414.95	34	57	1.66		67	1.77	1.595	V
Site 569 (Hole 569)										
1	1	1.02	52	75	1.43	12	78	1.59	1.541	V
2	1	2.22	55	76	1.38	15	81	1.54	1.523	V
2	3	5.32	53	74	1.40	16			1.534	V
2	5	8.42	57	77	1.35	22			1.504	V
3	2	13.31	53	74	1.40	19	80	1.55	1.542	V
3	4	16.31	49	71	1.44	17			1.532	V
4	1	20.81	52	74	1.41	18	81	1.53	1.526	V
4	4	25.31	55	76	1.38	22			1.516	V
4	6	29.12	47	69	1.46	19			1.546	V
5	1	31.02	55	75	1.38	19	80	1.55	1.507	V
5	3	34.02	51	73	1.42	38			1.515	V
6	2	42.77	52	73	1.40	12	86	1.45	1.525	V
6	4	44.82	51	73	1.42	37			1.530	V
6	6	48.32	49	71	1.44	33			2.104	V
7	1	51.02	52	73	1.39	15			1.535	V
7	4	55.52	51	72	1.40	33			1.694	V
7	6	58.32	45	67	1.51	55	73	1.67	1.492	V
8	2	60.92	41	64	1.56	18			1.762	V
8	3	62.82	46	68	1.49	48	75	1.63	1.874	V
9	2	70.92	50	71	1.44	65	85	1.47		
10	1	78.90	50			42	73	1.58	1.501	V
11	1	87.94	46			37	74	1.55		
11	2	90.26	48			53	71	1.61	2.177	V
12	1	98.50	46			52			1.450	V
12	3	100.38	50			37	87	1.44	1.568	V
12	6	105.59	45			53		1.32		
13	1	106.86	45	68	1.51			1.28	1.493	V
13	4	111.45	47	70	1.50				1.668	V
14	2	117.83	35	58	1.65		65	1.79	1.679	V
15	2	127.56	37	61	1.64		65	1.77	1.717	V
16	CC	136.33	33	56	1.69		72	1.68	1.760	V
17	5	151.26	37	60	1.65		66	1.79	1.681	V
17	6	152.66	40	63	1.59		68	1.75	1.560	V
18	2	156.78	39	63	1.63		66	1.79	1.673	V
20	1	174.32	37	60	1.64		64	1.83	1.737	V
21	1	184.22	33	57	1.71		59	1.88	1.724	V
22	2	194.52	32	56	1.73		67	1.76	1.559	V
23	1	203.47	34				65	1.80		
23	2	206.51	34	57	1.66		59	1.90	1.704	V
24	1	212.35	33	56	1.72		61	1.87	1.790	V
24	5	218.93	37	60	1.63		67	1.78	1.748	V
25	1	222.86	33	55	1.67		59	1.90	1.687	V

Appendix. (Continued).

Core	Section	Sub-bottom depth (m)	Water content (%)	Porosity (%)	Bulk density (Mg/m^3)	Un-drained shear strength (kPa)	2-min. GRAPE porosity (%)	2-min. GRAPE bulk density (Mg/m^3)	Compressional-wave velocity (km/s)	Direction[a]
(Hole 569 Cont.)										
26	1	231.77	35	58	1.66		65	1.79	1.797	V
26	5	238.41	35	58	1.66		64	1.81	1.697	V
27	3	245.22	33	57	1.71		59	1.86	1.791	V
Site 569 (Hole 569A)										
1	1	246.98	35	59	1.67		62	1.84	1.749	V
1	4	251.73	34	57	1.71		58	1.89	1.846	V
2	1	256.96	33	56	1.69		62	1.84	1.789	V
4	1	274.62	33	57	1.72		53	2.01	1.913	V
6	1	294.54	23	45	1.96		46	2.11	1.761	V
7	CC	304.74	31	55	1.76		53	2.00	1.969	V
9	1	332.32	12	27	2.19		23	2.50	2.680	V
9	CC	334.10	22	40	1.78		20	2.55	1.618	V
10	1	351.67			2.74				5.234	H
10	1	352.16					7	2.63	4.983	V
10	1	352.38			2.58				5.126	H
10	2	353.28						2.87		
Site 570 (Hole 570)										
1	1	1.02	51	73	1.43	8	77	1.61	1.580	V
1	2	2.52	47	70	1.48	15	74	1.65	1.566	V
1	3	4.32	47	69	1.48	33	75	1.63	1.570	V
2	1	5.92	46	68	1.49	10	77	1.59	1.550	V
2	3	8.12	45	68	1.50	20			1.577	V
2	5	10.92	44	65	1.50	33			1.576	V
3	2	19.52	42	64	1.50	13			1.504	V
3	5	24.52	42	64	1.53	35			1.809	V
3	6	25.52	39	62	1.58	46	69	1.73	1.742	V
4	1	28.22	42	64	1.52	21			1.795	V
4	4	32.01	39	62	1.59	47	70	1.71	1.811	V
5	6	45.72	43	65	1.51	7	73	1.67	1.895	V
6	2	48.17	44	64	1.47	18	75	1.64	1.601	V
6	4	52.02	44	65	1.50	14			1.558	V
6	6	54.92	42	63	1.52	63	81	1.54		
7	1	56.11	9	20	2.34		53	1.89		
7	2	58.82	40	62	1.56	61	69	1.73		
8	1	66.32	43	64	1.52	48	73	1.66		
8	3	68.92	40	63	1.58	52	67	1.76		
9	1	76.32	45	67	1.48	58	75	1.62		
10	2	87.42	42	64	1.52	44	73	1.66		
11	1	95.50	44	66	1.51	85	77	1.61		
11	3	98.56	41			25				
14	1	124.72	42	64	1.52	32	76	1.62		
14	5	130.15	44			36				
15	2	135.43	43			26	78	1.58	1.450	V
16	4	147.93	40	62	1.56		71	1.60		
16	6	150.81	35	57	1.62					
17	1	153.93	39	62	1.60	85	71	1.60		
17	5	159.43	38	61	1.59	96				
18	2	164.93	30	52	1.73	64				
19	1	172.11	14	31	2.16				2.674	V
19	3	176.43	36	59	1.62					
20	1	183.03	44	70	1.58	74				
21	2	194.00	76		1.55	83				
22	1	202.22	38	60	1.57	88				
22	4	206.23	37	60	1.61	73				
23	1	211.87	37	59	1.60	82				
23	4	216.32	38	60	1.58	60				
24	1	221.01	21	42	1.96	94	46	2.10	1.538	V
24	4	224.92	39	64	1.64		75	1.63	1.206	V
25	3	233.32	39	63	1.61		69	1.72		
26	4	244.19	44	63	1.44		77	1.60		
27	CC	250.70	7	18	2.40		18	2.57	2.625	V
28	7	268.12	42	62	1.47		76	1.61		
29	2	271.02	40	60	1.50		74	1.65		
30	4	283.47	48	67	1.46		75	1.63		V
31	1	288.98	40				81	1.53		V
32	5	303.92	37				72	1.61		V
34	2	319.02	39				70	1.65		V
35	2	327.83	31				62	1.74		V

Appendix. (Continued).

Core	Section	Sub-bottom depth (m)	Water content (%)	Porosity (%)	Bulk density (Mg/m^3)	Undrained shear strength (kPa)	2-min. GRAPE porosity (%)	2-min. GRAPE bulk density (Mg/m^3)	Compressional-wave velocity (km/s)	Direction[a]
(Hole 570 Cont.)										
37	2	347.62	7	17	2.41		21	2.51	3.994	V
39	1	365.61					30	2.24		
39	1	365.88					24	2.34	3.857	V
39	1	365.88							3.823	H
39	CC	366.04					23	2.51	3.601	V
41	1	383.87			2.31		19	2.45		
41	2	385.31	31	54	1.73		58	1.92		
41	3	386.97					18	2.46		
41	3	387.31			2.46		17	2.48	4.244	H
41	3	387.31							3.921	V
41	3	387.65			2.43		14	2.51	3.896	V
41	3	387.65							3.931	H
41	4	387.92					17	2.45		
42	1	392.92			2.45		14	2.51	4.015	V
42	1	393.32			2.42		16	2.55	3.714	V
42	2	394.43			2.40		17	2.45	3.815	V
42	3	396.94			2.32				3.958	V
42	3	396.94							4.265	H

[a] Direction of velocity measurement relative to upright core. V = vertical; H = horizontal.